Mapping and Assessing Variability in the Antarctic Marginal Ice Zone, the Pack Ice and Coastal Polynyas in two Sea Ice Algorithms with implications on Breeding Success of Snow Petrels

Julienne C. Stroeve[1,2], Stephanie Jenouvrier[3,4], G. Garrett Campbell[1], Christophe Barbraud[4] and Karine Delord[4]

[1]National Snow and Ice Data Center, Cooperative Institute for Research in Environmental Sciences, University of Colorado, Boulder, CO, USA

[2]Center for Polar Observation and Modelling, University College London, London, UK

[3]Woods Hole Oceanographic Institution, Woods Hole, MA, USA

[4]Centre d'Etudes Biologiques de Chizé, UMR 7372 CNRS, 79360 Villiers en Bois, France

Abstract

Sea ice variability within the marginal ice zone (MIZ) and polynyas plays an important role for phytoplankton productivity and krill abundance. Therefore, mapping their spatial extent, seasonal and interannual variability is essential for understanding how current and future changes in these biologically active regions may impact the Antarctic marine ecosystem. Knowledge of the distribution of MIZ, consolidated pack ice and coastal polynyas to the total Antarctic sea ice cover may also help to shed light on the factors contributing towards recent expansion of the Antarctic ice cover in some regions and contraction in others. The long-term passive microwave satellite data record provides the longest and most consistent record for assessing the proportion of the sea ice cover that is covered by each of these ice categories. However, estimates of the amount of MIZ, consolidated pack ice and polynyas depends strongly on what sea ice algorithm is used. This study uses two popular passive microwave sea ice algorithms, the NASA Team and Bootstrap, and applies the same thresholds to the sea ice concentrations to evaluate the distribution and variability in the MIZ, the consolidated pack ice and coastal polynyas. Results reveal that the seasonal cycle in the MIZ and pack ice is generally similar between both algorithms, yet the NASA Team algorithm has on average twice the MIZ and half the consolidated pack ice area as the Bootstrap algorithm. Trends also differ, with the Bootstrap algorithm suggesting statistically significant trends towards increased pack ice area and no statistically significant trends in the MIZ. The NASA Team algorithm on the other hand indicates statistically significant positive trends in the MIZ during spring. Potential coastal polynya area and broken ice within the consolidated ice pack is also larger in the NASA Team algorithm. The timing of maximum polynya area may differ by as much as 5 months between algorithms. These differences lead to different relationships between sea ice characteristics and biological processes, as illustrated here with the breeding success of an Antarctic seabird.

1. Introduction

Changes in the amount of the ocean surface covered by sea ice play an important role in the global climate system. For one, sea ice and its snow cover have a high surface reflectivity, or albedo, reflecting the majority of the sun's energy back to space. This helps to keep the polar regions cool and moderates the global climate. When sea ice melts or retreats, the darker (lower albedo) ocean is exposed, allowing the ocean to absorb solar energy and warm, which in turn melts more ice, creating a positive feedback loop. During winter, sea ice helps to insulate the ocean from the cold atmosphere, influencing the exchange of heat and moisture to the atmosphere with impacts on cloud cover, pressure distribution and precipitation. These in turn can lead to large-scale atmospheric changes, affecting global weather patterns [e.g. *Jaiser et al.*, 2012]. Sea ice also has important implications for the entire polar marine ecosystem, including sea ice algae, phytoplankton, crustaceans, fish, seabirds, and marine mammals, all of which depend on the seasonal cycle of ice formation in winter and ice melt in summer. For example, sea ice melt stratifies the water column, producing optimal light conditions for stimulating bloom conditions. Antarctic sea birds rely upon the phytoplankton bloom for their breeding success and survival [e.g. *Park et al*., 1999].

In stark contrast to the Arctic, which is undergoing a period of accelerated ice loss [e.g. *Stroeve et al*., 2012; *Serreze and Stroeve*, 2015], the Antarctic is witnessing a modest increase in total sea ice extent [*Parkinson and Cavalieri*, 2012; *Simmonds et al*., 2015]. Sea ice around Antarctica reached another record high extent in September 2014, recording a maximum extent of more than 20 million km^2 for the first time since the modern passive microwave satellite data record began in October 1978. This follows previous record maxima in 2012 and 2013 [*Reid et al*., 2015], resulting in an overall increase in Antarctic September sea ice extent of 1.1% per decade since 1979. While the observed increase is statistically significant, Antarctic's sea ice extent (SIE) is also highly variable from year to year and region to region [e.g. *Maksym et al*., 2012; *Parkinson and Cavalieri*, 2012; *Stammerjohn et al*., 2012]. For example, around the West Antarctic Peninsula (WAP), there have been large decreases in sea ice extent and sea ice duration [e.g. *Ducklow et al*., 2012; *Smith and Stammerjohn*, 2001], coinciding with rapid warming since 1950 [*Ducklow et al*., 2012].

The temporal variability of the circumpolar Antarctic sea ice extent is underscored by sea ice conditions in 2015 when the winter ice cover returned back to the 1981-2010 long-term mean. Also, recent sea ice assessments from early satellite images from the Nimbus program of the late 1960s indicate similarly high but variable SIE as observed over 2012-2014 [*Meier et al.,* 2013; *Gallaher et al.,* 2014]. Mapping of the September 1964 ice edge indicates that ice extent likely exceeded both the 2012 and 2013 record monthly-average maxima, at 19.7±0.3 million km^2. This was followed in August 1966 by an extent estimated at 15.9±0.3 million km^2, considerably smaller than the record low maximum extent of the modern satellite record (set in 1986). The circumpolar average also hides contrasting regional variability, with some regions showing either strong positive or negative trends with magnitudes equivalent to those observed in the Arctic [*Stammerjohn et al*., 2012]. In short, interannual and regional variability in Antarctic sea ice is considerable, and while the current positive trend in circumpolar averaged Antarctic sea ice extent is important, it is not unprecedented compared to observations from the 1960s and it is not regionally distributed.

Several explanations have been put forward to explain the positive Antarctic sea ice trends. Studies point to anomalous short-term wind patterns that both grow and spread out the ice, related to the strength of the Amundsen Sea low pressure [e.g. *Turner et al.,* 2013; *Reid et al*., 2015; *Holland and Kwok*, 2012]. Other studies suggest melt water from the underside of floating ice surrounding the continent has risen to the surface and contributed to a slight freshening of the surface ocean [e.g. *Bintanja et al*., 2013]. While these studies have helped to better understand how the ice, ocean and atmosphere interact, 2012 to 2014 showed different regions and seasons contributing to the net positive sea ice extent, which has made it difficult to establish clear links and suggests that no one mechanism can explain the overall increase.

While the reasons for the increases in total extent remain poorly understood, it is likely that these changes are not just impacting total sea ice extent but also the distribution of pack ice, the marginal ice zone (MIZ) and polynyas. The MIZ is a highly dynamic region of the ice cover, defined by the transition between the open ocean and the consolidated pack ice. In the Antarctic, wave action penetrates hundreds of kilometers into the ice pack, resulting in small rounded ice floes from wave-induced fracture [*Kohout et al.,* 2014]. This in turn makes the MIZ region particularly sensitive to both atmospheric and oceanic forcing, such that during quiescent conditions, it may consist of a diffuse thin ice cover, with isolated thicker ice floes distributed over a large (hundreds of kilometers) area. During high on-ice wind and wave events, the MIZ region contracts to a compact ice edge with rafted ice pressed together in front of the solid ice pack. The smaller the ice floes, the more mobile they are and large variability in ice conditions can be found in response to changing wind and ocean conditions. Polynyas on the other hand are open water areas near the continental margins [e.g. *Morales-Maqueda et al*., 2004] that often remain open as a result of strong katabatic winds flowing down the Antarctic plateau. The winds continuously push the newly formed sea ice away from the continent, which influences the outer ice edge as well, thus contributing to the overall increase in total ice extent in specific regions around the Antarctic continent where katabatic winds are persistent.

Both polynyas and the MIZ are biologically important regions of the sea ice cover that have implications for the entire trophic web, from primary productivity [*Yun et al*., 2015], to top predator species, such as seabirds. Near the ice edge and in the MIZ, the stable upper layer of the water column is optimal for phytoplankton production [e.g. *Park et al*., 1999]. This phytoplankton bloom is subsequently exploited by zooplankton, with effects that cascade up to fish, seabirds and marine mammals. Similarly, within polynyas there is a narrow opportunity for phytoplankton growth, the timing of which plays an important role in both biogeochemical cycles [*Smith and Barber*, 2007] and biological production [*Arrigo and van Dijken*, 2003; *Ainley et al*., 2010]. However, while studies have suggested that the timing of sea ice retreat is synchronized with the timing of the phytoplankton bloom, other factors such as wind forcing [*Chiswell*, 2011], thermal convection [*Ferrari et al.,* 2014] and iron availability [*Boyd et al*, 2007, and references therein] play important roles as well.

In this study we use the long-term passive microwave sea ice concentration data record to evaluate variability and trends in the MIZ, the pack ice and polynyas from 1979 to 2014. A complication arises however as to which sea ice algorithm to use. There are at least a dozen algorithms available, spanning different time-periods, which give sea ice concentrations that are not necessarily consistent with each other [*see Ivanova et a*l., 2015; 2014 for more information]. To complicate matters, different studies have used different sea ice algorithms to examine sea ice variability and attribution. For example, *Hobbs and Raphael* [2010] used the Had1SST1 sea ice concentration data set [*Rayner et al.,* 2003], which is based on the NASA Team algorithm [*Cavalieri et al*., 1999], whereas *Raphael and Hobbs* [2014] relied on the Bootstrap algorithm [*Comiso and Nishio*, 2008]. To examine the influence in the choice of sea ice algorithm on the results, we use both the Bootstrap (BT) and NASA Team (NT) sea ice algorithms. Results are evaluated hemispheric-wide and also for different regions. We then discuss the different implications resulting from the two different satellite estimates for biological impact studies. We focus on the breeding success of snow petrels because seabirds have been identified as useful indicators of the health and status of marine ecosystems [*Piatt and Sydeman*, 2007].

2. Data and Methods

To map different ice categories, the long-term passive microwave data record is used, which spans several satellite missions, including the Scanning Multichannel Microwave Radiometer (SMMR) on the Nimbus-7 satellite (October 1978 to August 1987), the Special Sensor Microwave/Imager (SSM/I) sensors -F8 (July 1987 to December 1991), -F11 (December 1991 to September 1995), -F13 (May 1995 to December 2007) and the Special Sensor Microwave Imager/Sounder (SSMIS) sensor –F17 (January 2007- to present), both on the Defense Meteorological Satellite Program's (DMSP) satellites. Derived sea ice concentrations (SICs) from both the Bootstrap [*Comiso and Nishio*, 2008] and the NASA Team [*Gloersen et al.,* 1992; *Cavalieri et al.,* 1999] are available from the National Snow and Ice Data Center (NSIDC) and provide daily fields from October 1978 to present, gridded to a 25 km polar stereographic grid. While a large variety of SIC algorithms are available, the lack of good validation has made it difficult to determine which algorithm provides the most accurate results during all times of the year and for all regions. Using two algorithms provides a consistency check on variability and trends. Note that NSIDC has recently combined these two algorithms to build a climate data record (CDR) [*Meier et al.,* 2013].

Using these SIC fields, we define six binary categories of sea ice based on different SIC thresholds [**Table 1**]. Because the marginal ice zone is highly dynamic in time and space, it is difficult to precisely define this region of the ice cover. *Wadhams* [1986] defined the MIZ as that part of the ice cover close enough to the open ocean boundary to be impacted by its presence, e.g. by waves. Thus the MIZ is typically defined as the part of the sea ice that is close enough to the open ocean to be heavily influenced by waves, and it extends from the open ocean to the dense pack ice. In this study, we define the MIZ as extending from the outer sea ice/open ocean boundary (defined by SIC $\geq$ 0.15 ice fraction) to the boundary of the consolidated pack ice (defined by SIC = 0.80). This definition was previously used by *Strong and Rigor* [2013] to assess MIZ changes in the Arctic and matches the upper SIC limit used by the National Ice Center in mapping the Arctic MIZ. The consolidated ice pack is then defined as the area south of the MIZ with ice fractions between 0.80 $\leq$ SIC $\leq$ 1.0. Potential coastal polynyas are defined as regions near the coast that have SIC < 0.80.

To automate the mapping of different ice categories, radial transects from 50 to 90S are individually selected to construct one-dimensional profiles [**Figure 1**]. The algorithm first steps from the outer edge until the 0.15 SIC is detected, providing the latitude of the outer MIZ edge. Next, the algorithm steps from the outer MIZ edge until either the 0.80 SIC is encountered, or the continent is reached. Data points along the transect between these SIC thresholds are flagged as the MIZ. In this way, the MIZ includes an outer band of low sea ice concentrations that surrounds a band of inner consolidated pack ice, *but* sometimes the MIZ also extends all the way to the Antarctic coastline (as sometimes observed in summer). South of the MIZ, the consolidated ice pack (0.80 $\leq$ SIC $\leq$ 1.0) is encountered; however, low sea ice concentrations can appear near the coast inside the pack ice region as well. These are areas of potential coastal polynyas. While it is difficult to measure the fine scale location of a polynya at 25km spatial resolution, the lower sea ice concentrations provide an indication of some open water near the coast, which for sea birds provides a source of open water for foraging. We have previously tested mapping polynyas using a SIC threshold of 0.75 and 0.85 for the NASA Team and Bootstrap algorithms, respectively, and found that these thresholds provided consistent polynya areas between the two algorithms and matched other estimates of the spatial distribution of polynyas [see *Li et al.,* 2016]. However, for this study we chose just one threshold, a compromise between the two algorithms, so that we can better determine the sensitivity of using the same threshold on polynya area and timing of formation.

Using our method of radial transects, the algorithm then steps from the coast northward and flags pixels with < 0.80 SIC until a 0.80 SIC pixel appears and defines that region as a potential coastal polynya. Within the consolidated pack ice (and away from the coast), it is also possible to encounter instances where 0.15 < SIC < 0.80 or SIC < 0.15. These are flagged as open pack ice and open water areas within the consolidated pack ice, respectively. Finally, an ocean mask derived from climatology and distributed by NSIDC was applied to remove spurious ice concentrations at the ice edge as a result of weather effects.

Figure 2 shows sample images of the classification scheme as applied to the NASA Team and Bootstrap algorithms on days 70 (March 11) and 273 (September 30), respectively, in 2013. During the fall and winter months when the ice cover is expanding there is a well-established consolidated pack ice region, surrounded by the outer MIZ. Coastal polynyas are also found surrounding the continent in both algorithms. The BT algorithm tends to show a larger consolidated ice pack than NT, particularly during the timing of maximum extent. During the melt season there is mixing of low and high ice concentrations, leading to mixtures of different categories, which is still seen to some extent in the March images. However, during March areas of polynyas (green), open water (pink) and open pack ice (orange) appear to extend from the coastline in some areas (e.g. southern Weddell and Ross seas). While any pixel with SIC < 0.8 adjacent to the coastal boundary is flagged as potential polynya when stepping northwards, if a pixel is already flagged as MIZ or consolidated pack ice when stepping southwards, it remains flagged as MIZ or pack ice. After that analysis, a check for pixels with SICs less than 0.8 is done to flag for broken ice or open water. Thus, during these months (e.g. December to February or March), the physical interpretation of the different ice classes may be less useful.

Using the binary classification scheme, daily gridded fields at each 25 km pixel are obtained. Using this gridded data set we then obtain regional averages for five different regions as defined previously by *Parkinson and Cavalieri* [2012]. These regions are shown in **Figure 3** for reference. Climatological mean daily and monthly time-series spanning 1981 to 2010 are computed for each of the five sub-regions, as well as the entire circumpolar region, and for each ice classification together with the +/- one standard deviation (1σ). Monthly trends over the entire time-series are computed by first averaging the daily fields into monthly values and then using a standard linear least squares, with statistical significance evaluated at the 90^{th}, 95^{th} and 99^{th} percentiles using a student t-test.

3. Results

3.1 Seasonal Cycle

3.1.1 Circumpolar Extent

We begin with an assessment of the consistency of the outer ice edge between both sea ice algorithms [**Figure 4**]. As a result of the large emissivity difference between open water and sea ice, estimates of the outer ice edge location has high consistency between the two algorithms despite having large differences in SIC [e.g. *Ivanova et al*., 2014; 2015]. This results in similar total sea ice extents between both algorithms during all calendar months, except for a small southward displacement of the Bootstrap ice edge during summer, and similar long-term trends. This is where the similarities end however.

Figure 5 summarizes the climatological mean seasonal cycle in the extent of the different ice categories listed in Table 1 for both sea ice algorithms, averaged for the total hemispheric-wide Antarctic sea ice cover. The one standard deviation is given by the colored shading. The first notable result is that the BT algorithm has a larger consolidated ice pack than the NT algorithm, which comes at the expense of a smaller MIZ. Averaged over the entire year, the NT MIZ area is twice as large as that from BT [see also **Table 2**]. The BT algorithm additionally has a smaller spatial extent of potential coastal polynyas and little to no broken ice or open water within the consolidated pack ice. Another important result is that the BT algorithm exhibits less interannual variability in the 5 ice categories identified, as illustrated by the smaller standard deviations from the long-term mean. Thus, while the total extents are not dissimilar between the algorithms, how that ice is distributed among the different ice categories differs quite substantially as well as their year-to-year variability.

The timing of the ice edge advance and retreat are generally similar, reflecting the fact that both algorithms do well in distinguishing open water from sea ice. In regards to the consolidated pack ice, it advances in March, with the BT algorithm showing a distinct peak in September, reaching a maximum extent of 14.89 10^6 km^2. The NT algorithm shows a somewhat broader peak, extending from July to October, with the peak extent also reached in September. In September the NT pack ice extent is a little more than twice the spatial extent of the MIZ; 11.31 10^6 km^2 vs. 5.41 10^6 km^2 [Table 2]. BT on the other hand has a much smaller fraction (41% less) of ice classified as MIZ (3.19 10^6 km^2). In both algorithms the MIZ also begins to expand in March, and continues to expand until November or December, after which it rapidly declines. However, in the NT algorithm, an initial peak in MIZ coverage is also reached around September, coinciding with the peak in the consolidated pack ice extent and stays nearly constant until the end of November. The further increase in the MIZ coverage after the consolidated ice pack begins to retreat implies that as the pack ice begins to retreat, it does so in part by first converting to MIZ over a wider area. This is consistent with the idea that in spring, the pack ice on average undergoes divergence first (in relation to the circumpolar trough being poleward and south of the ice edge, as reflected by the Semi-Annual Oscillation, SAO, of the trough). This in turn facilitates increased solar heating of open water areas, which in turn facilitates increased melt back, thus creating, eventually, a more rapid ice edge retreat (in Nov-Dec) as compared to the slow ice edge advance in autumn [see *Watkins and Simmonds*, 1999].

Open pack ice is negligible in the Bootstrap algorithm except for a slight peak in November/December. With the NASA Team algorithm however there is a clear increase in open pack ice during the ice expansion phase, which continues to increase further as the pack ice begins to retreat, also peaking in November. Open pack ice in September contributes another 1.28 10^6 km^2 to the total Antarctic sea ice extent in the NT algorithm, compared to only 0.36 10^6 km^2 in the BT algorithm. As with the open pack ice, the fraction of potential coastal polynyas also increases during the ice expansion phase, and then continues to increase as the sea ice retreats, peaking around November in the NT algorithm, with a total area of 1.02 10^6 km^2, and in December in BT (0.81 10^6 km^2). Inner open water within the pack is generally only found between November and March in both algorithms as the total ice cover retreats and reaches its seasonal minimum.

3.2.2 Regional Analysis

Analysis of the Antarctic-wide sea ice cover however is of limited value given that the sea ice variability and trends are spatially heterogeneous [*Makysm et al.*, 2012]. For example, while the ice cover is increasing in the Ross Sea, it has at the same time decreased in the

Bellingshausen/ Amundsen Sea region. Thus, we may anticipate significant regional variability in the amount, seasonal cycle and trends of the different ice classes (trends discussed in section 3.3). The Ross Sea for example [**Figure 6, top**] consists of a large fraction of consolidated ice throughout most of the year (April through November) in both algorithms, with considerably less MIZ. In the Bellingshausen/Amundsen (B/A) Sea on the other hand [**Figure 6, 2nd row**], the NT algorithm has a MIZ extent that exceeds that of the consolidated pack ice until May, after which the spread (+/- 1σ) in MIZ and consolidated pack ice overlaps. The reverse is true in the BT algorithm, which consistently indicates a more consolidated ice pack, with only 0.51 10^6 km^2 flagged as MIZ during the maximum extent in September, compared to 0.84 10^6 km^2 in the NT algorithm. On an annual basis, the NT algorithm shows about equal proportion of MIZ and consolidated pack ice in the B/A Sea whereas, the BT algorithm indicates a little more than a third of the total ice cover is MIZ. Note also that the B/A Sea is the only region where the maximum MIZ extent does not occur after the maximum pack ice extent during spring. This is true for both sea ice algorithms.

In the Ross Sea there is also a very broad peak in the maximum extent of the consolidated pack ice, stretching between July and October in the NT algorithm, and a peak in MIZ extent in late August/early September with a secondary peak in December as the pack ice continues to retreat. The BT algorithm shows a similar broad peak in the pack ice extent, but with less interannual variability, and a nearly constant fraction of MIZ throughout the advance and retreat of the pack ice. Annually the NT algorithm shows about 56% more MIZ in the Ross Sea than the BT algorithm. Note that in both algorithms, the pack ice retreats rapidly after the maximum extent is reached.

In the Weddell Sea, the pack ice extent advances in March in both algorithms and peaks in August in the NT algorithm, September in BT. The MIZ also begins its expansion in March and continues to increase until September in NT, and then again until December (both algorithms) as the pack ice quickly retreats [**Figure 6 (middle)**]. In this region, the sea ice expands northwards until it reaches a region with strong winds and currents. The open pack ice north of the pack ice continues to expand either by further freezing or breaking of the pack ice by the winds and currents. Overall, the Weddell Sea has the largest spatial extent in the MIZ in both algorithms, as well as the largest distribution of pack ice. In the NT algorithm, the MIZ extent within the Weddell Sea is again larger than in the BT algorithm and has considerably larger interannual variability. For example, in September the NASA Team algorithm gives a climatological mean MIZ extent of 1.61 10^6 km^2, twice as large as that in the Bootstrap algorithm (0.83 10^6 km^2).

Finally, in the Indian and Pacific Ocean sectors [**Figure 6, 4th row and bottom**] the MIZ extent increases from March until November in both algorithms, retreating about a month after the peak extent in the pack ice is reached. However, in the Pacific Ocean sector, the NT MIZ comprises a larger percentage of the overall ice cover, being nearly equal in spatial extent, and even exceeding that of the pack ice in September (0.93 (MIZ) vs. 0.76 10^6 km^2 (pack ice)). This results in an annual mean extent of MIZ that exceeds that of the consolidated pack ice. This is the only region of Antarctica where this occurs. In the BT algorithm, the reverse is true, with again a larger annual extent of pack ice than MIZ.

While the above discussion focused on regional differences in the MIZ and the consolidated pack ice, the spatial extent and timing of coastal polynyas also varies between the algorithms. For example, in the B/A sea region, the maximum polynya area occurs in July in NT (0.17 10^6 km^2) and in December in the BT algorithm (0.11 10^6 km^2). Thus, while the overall maximum spatial extent in polynya area is not all that different in the two algorithms, the timing of when the maximum is reached differs by 5 months. This is also the case in the Pacific Ocean where the NT algorithm reaches its largest spatial extent in polynya area in August (0.14 10^6 km^2) whereas BT shows the maximum polynya area occurring in November (0.11 10^6 km^2). In other regions, such as the Indian Ocean, the Ross Sea and the Weddell Sea, the timing of the maximum polynya area occurs similarly in both algorithms, during November for the Indian Ocean and December in the Ross and Weddell Seas. The Ross and Weddell seas have the largest climatological polynya areas, 0.32 (NT)/0.26 (BT) 10^6 km^2 and 0.33 (NT)/0.30 (BT) 10^6 km^2, respectively.

3.2 Trends

3.2.1 Spatial Expansion/Contraction during September

As mentioned earlier, estimates of the outer ice edge location are similar between both algorithms. This is also true in terms of the locations where the outer edge is expanding or contracting. A way to illustrate this is shown in **Figure 7 (top)**, which shows a spatial map of the trend in the outer edge of the entire ice pack (defined as the 15% SIC contour, equivalent to the total sea ice extent) for both algorithms during the month of September, the month at which the ice pack generally reaches its maximum extent. Locations of northward expansion (red areas) and contraction (blue areas) are remarkably consistent between algorithms as well as the spatial extent of the expansion and contraction. In both algorithms the ice edge shows trends towards expansion within the Ross Sea, the Amundsen Sea and the Pacific and Indian Ocean sectors, except for the Davis Sea, where there is a trend towards contraction of the outer ice edge. The Bellingshausen and Weddell seas also show trends towards contraction of the outer ice edge.

While there is general consistency between the algorithms in both the location and changes of the outer ice edge over time, there are differences as to how the MIZ and pack ice widths are changing [**Figure 7, middle and bottom**]. The BT MIZ width is a relatively constant ring around the edge of the consolidated pack ice, with little change over time. Thus, in the BT algorithm, the spatial pattern of expansion/contraction of the total ice cover in September is largely a result of the changes happening in the pack ice [Figure 7, bottom]. The NT algorithm on the other hand shows more pronounced changes in the MIZ, such that both the MIZ and the pack ice contribute to the observed spatial patterns and changes in the total ice cover. However, expansion/contraction of the NT MIZ and pack ice sometimes counter act each other. For example the contraction of the total ice edge the Bellingshausen Sea is a result of contraction of the consolidated ice pack while the MIZ width is generally increasing as a result of the MIZ moving further towards the continent. This is also true in the Weddell Sea and the Indian Ocean.

Somewhat surprisingly, the spatial pattern of expansion/contraction of the MIZ is broadly similar between both algorithms, despite overall smaller changes in the BT algorithm. This highlights the fact that the spatial trends in SIC are similar to the spatial trends in SIE as well as to the timing of advance/retreat/duration, so that the spatial trends in the MIZ and pack ice will show the same overall pattern because they rely on SIC. This also highlights the fact that the spatial pattern persists throughout the regional ice covered area, i.e. from the edge to the coastal area, which may imply that climate-related regional wind-driven changes at the ice edge are felt all the way to the coast. Alternatively it may imply that the ocean is also responding to the same climate-related wind changes, thus communicating the change all the way to the coast.

3.2.2 Circumpolar and Regional Daily Trends

Figure 8 summarizes daily circumpolar Antarctic trends in the extent of pack ice, MIZ and polynyas for both algorithms, with monthly mean trends listed in **Table 3**. Both algorithms are broadly similar during the ice expansion phase, indicating positive trends in the consolidated ice pack and mostly negative trends in the MIZ until the pack ice reaches its peak extent. Thus, during these months, the positive trends in total SIE are a result of expansion of the consolidated pack ice. However, during retreat of the pack ice, trends in the NT MIZ switch to positive in the while remaining mostly negative in the BT algorithm. At the same time, daily trends in the pack ice become noisy in the NT algorithm, alternating between positive and negative trends while BT trends remain positive. Table 3 indicates that the positive trends in the consolidated pack during the ice expansion/retreat phase (March through November) are statistically significant ($p<0.01$) for the BT algorithm, and from March to July in the NT algorithm ($p<0.05$). Trends in the NT MIZ are not statistically significant, except during September and October ($p<0.10$). Trends in the pack ice are larger in the BT algorithm, particularly in August through November, in part reflecting a shrinking MIZ whereas the NT algorithm shows positive trends in the MIZ during those months. Trends in possible polynyas near the continent are negative throughout most of the year in both algorithms, except for December and January. However, none of the polynya trends are statistically significant.

Regionally, there are larger differences between the two algorithms. **Figure 9** shows monthly trends as a function longitude (x-axis) and month (y-axis) for the pack ice (top) and MIZ (bottom). Monthly trends averaged for each of the 5 sectors are also listed in Table 3. Focusing first on the pack ice trends, we find the spatial patterns of statistically significant positive and negative trends are generally consistent between both algorithms, though the magnitudes of the trends tend to be larger in the Bootstrap algorithm. For example, in the Ross Sea, the sign of the pack ice trends are spatially consistent between both algorithms, though not all trends are statistically significant, particularly for the NT algorithm. The largest consistency occurs in the the western Ross Sea, where positive trends are seen in both algorithms, statistically significant from March to November ($p<0.01$) in the BT algorithm, and from January to July and October to November in the NT algorithm. Note also that both algorithms show statistically significant positive trends in the MIZ from January to March in the western Ross Sea and generally negative trends in the eastern Ross Sea. This pattern switches from June to December, with mostly negative MIZ trends in the western Ross Sea and positive trends in the eastern Ross Sea. In particular, the statistically significant positive trends in the MIZ in the NT algorithm occur at the time of year with the largest overall trends in the SIE in this region. This would suggest perhaps different interpretation of processes impacting the overall ice expansion in the Ross Sea depending on which algorithm is used.

In the B/A Sea, statistically significant positive trends in pack ice are limited to May through August in the NT algorithm and June and July in the BT algorithm. The positive NT pack ice trends are offset by negative trends in the NT MIZ. Both algorithms exhibit negative pack ice trends during other months that are consistent between the algorithms, though larger in magnitude for the BT algorithm. This is generally compensated by statistically significant negative trends in the NT MIZ to give an overall negative decline of total extent.

Trends in the pack ice are also consistent between algorithms in the Weddell Sea, with statistically significant trends generally occurring at the same longitude and during the same months. The positive pack ice trends in MAM (NT) or MAMJ (BT) are confined to a very narrow longitude band which moves to the east with progressing season. Then in June, and continuing for several months, negative pack ice trends occur. For both algorithms, trends in the MIZ are generally not statistically significant, except for some positive trends in the eastern

Weddell Sea from January to March and negative trends mostly from June to November near 330 degrees longitude.

Finally, in the Pacific and Indian Oceans we again see spatial consistency in pack ice and MIZ trends for both algorithms, with generally larger (smaller) pack ice (MIZ) trends for the BT algorithm, though trends are closer in magnitude in the Pacific sector from March to July. Pack ice trends are generally positive, more in BT than NT and trends in MIZ extent basically vary around zero with exceptions during August through December in both algorithms in the Pacific Ocean.

In summary, while the magnitude of trends differs between both algorithms, there is general spatial consistency in the patterns of positive and negative trends in the consolidated pack ice and the MIZ. Results suggest that positive trends in total SIE are generally a result of statistically significant positive trends in the consolidated pack ice in the BT algorithm in all sectors of the Antarctic, except for the Bellingshausen/Amundsen Sea sector and the Weddell Sea during ice retreat. The NT algorithm on the other hand suggests more instances of statistically significant positive trends in the MIZ, though this is highly regionally dependent.

3.2.3 Seasonal Trends in MIZ and Pack Ice Width

Finally, we compute the overall width of the MIZ and pack ice following *Strong and Rigor* [2013] and produce seasonal means. Briefly, following the classification of each ice category, latitude boundaries are computed for each longitude and each day. These are averaged for each month to provide monthly mean latitude boundaries at each longitude. The boundaries are subsequently converted to width in km, and averaged for all longitudes. Finally, seasonal means are derived.

Time-series of seasonal means of the circumpolar MIZ width and pack ice width are shown in **Figure 10** for all seasons except summer when the results are noisy. As we may expect following the previous results, the NT MIZ width is larger and the pack ice width is smaller than the seen in the BT algorithm. During autumn (MAM) however, the differences in widths for both the MIZ and the pack ice between the algorithms are largely reduced compared to the other seasons. For example the difference in 1979-2014 pack ice width between the algorithms during MAM is 60 km, 121 km in JJA and 139 km in SON. Similarly, the long-term mean MIZ width differences are 54 km (MAM), 74 km (JJA) and 83 km (SON). In addition, during autumn, trends in the MIZ and pack ice are largely consistent between the two algorithms, with no trend in the MIZ and increases in the pack ice on the order of 21.2 km dec^{-1} and 20.0 km dec^{-1} ($p<0.01$) for the BT and NT algorithms, respectively. This is the season with the largest trends in the pack ice width, representing a 21% widening over the satellite record.

During winter (JJA) and spring (SON) however, the NT and BT algorithms exhibit opposing trends in the MIZ with the NT algorithm indicating an increase, and the BT a decrease. The largest positive trend in the MIZ width occurs during spring at a rate of +10.3 km dec^{-1} ($p<0.01$) in the NT algorithm, indicating a 6% widening since 1979. This widening is a result of the MIZ moving slightly equatorward rather than expanding southwards (as also seen in Figure 7). However, this is an increase of only about 1 to 1.5 grid cells over the entire data record, and despite a statistically significant trend, there remains substantial interannual variability in the SON MIZ width, with the maximum width recorded in 2003 (310 km) and the minimum in 1985 (217 km), with a mean SON MIZ width of 248 km. The trend during winter is considerably smaller at +2.7 km dec^{-1}, as a result of expansion both equatorward and southwards, yet it is not statistically significant.

For the pack ice, both sea ice algorithms show statistically significant positive trends towards increased width of the pack ice, which are also nearly identical during winter at +18.7 and +18.1 km dec^{-1} ($p<0.01$) for the BT and NT algorithms, respectively. This represents a widening of the pack ice of approximately 11% from 1979 to 2014 during winter. As one may expect, differences in the pack ice width between the algorithms are largely found in spring as a result of the MIZ expanding in the NT algorithm. Therefore, during SON the trends in the width of the NT pack ice are smaller, with trends of +10.0 ($p<0.05$) km dec^{-1} compared to +16.7 ($p<0.01$) for the BT algorithm.

Finally it is important to point out that the interannual variability in the pack ice is similar between both data sets despite differences in magnitude. Correlations between the two algorithms are: 0.96 (MAM), 0.92 (JJA) and 0.77 (SON). The reason for the weaker correlation in SON is not entirely clear. For the MIZ, interannual variability is generally about twice as large in the NASA Team algorithm and the two data sets are not highly correlated except for autumn, with correlations of 0.67 (MAM), 0.39 (JJA) and 0.43 (SON).

4. Implications for a Seabird

Here we use data on the MIZ and the consolidated ice pack from both algorithms to understand the role of sea ice habitat on breeding success of a seabird, the snow petrel *Pagodroma nivea*. As mentioned in the introduction, the MIZ is a biologically important region because it is an area of high productivity and provides access to food resources needed by seabirds [*Ainley et al*., 1992]. During winter, productivity is reduced at the surface in open water, while it is concentrated within the ice habitat, especially within the ice floes [*Ainley et al.,* 1986]. This patchy distribution of food availability within the MIZ and pack ice provides feeding opportunities for seabirds such as the snow petrel. Observations suggest that the snow petrel forages more successfully in areas close to the ice edge and within the MIZ than in consolidated ice conditions [*Ainley et al.,* 1984, 1992].

Breeding success of snow petrels depends on sufficient body condition of the females, which in part reflects favorable environmental and foraging conditions prior to the breeding season. Indeed, female snow petrels in poor early body condition are not able to build up the necessary body reserves for successful breeding [*Barbraud and Chastel*, 1999]. Breeding success was found to be higher during years with extensive sea ice cover during the preceding winter [*Barbraud and Weimerskirch*, 2001]. This is in part because winters with extensive sea ice are associated with higher krill abundance the following summer [*Flores et al*., 2012; *Loeb et al.,* 1997; *Atkinson et al.,* 2004], thereby increasing the resource availability during the breeding season. However, extensive winter sea ice may protect the under ice community from predation and thus reduce food availability, in turn affecting breeding success [*Olivier et al.,* 2005]. By distinguishing between the areas of MIZ and pack ice, we can expect a better understanding of the role of sea ice on food availability and hence breeding success of snow petrels.

In the following, we expect that an extensive pack ice during winter may reduce breeding success the following breeding season by protecting the under ice community from predation, while an extensive MIZ may increase breeding success by providing easier access to foraging. With the classifications as defined by both algorithms we calculated the MIZ and pack ice area in a wide rectangular sector defined by the migration route of the snow petrel [*Delord et al.,* 2016] from April to September [see **Table 4** for latitude and longitude limits]. This is the first time that appropriate areas of the observed foraging range are used to study the carry over effect of winter conditions on the breeding performance of snow petrel, as this information did not existed previously. Using these locations, we averaged the MIZ and pack ice extents over the entire winter from April to September. We next employed a logistic regression approach to study the effects of MIZ and pack ice area within this sector and evaluate the impacts on breeding success the following summer. The response variable was the number of chicks C_t in a breeding season *t*, from 1979 to 2014 collected at Terre Adélie, Dumont D'Urville [*Barbraud and Weimerskirch*, 2001, *Jenouvrier et al*., 2005].

Effects of MIZ and pack ice area were analyzed using Generalized Linear Models (GLM) with logit-link functions and binomial errors fitted in R using the package glm. Specifically, the response variable is the number of chicks C_t in a breeding season *t*, from 1979 to 2014 collected at Terre Adelie, Dumont D'Urville [*Barbraud and Weimerskirch*, 2001, *Jenouvrier et al*., 2005]. It follows a binomial distribution, such that $C_t \sim Bin(\mu_t, N_t)$, where N_t is the number of breeding pairs and μ_t is the breeding success in year *t*. The breeding success is a function of the MIZ and pack ice covariates at time *t* (COV) such as:

$$\mu_t = \beta_0 + \beta_1\, COV_{(t)}$$

To select the covariate that most impacts the breeding success of snow petrels, we applied the information-theoretic (I-T) approaches [*Burnham et al*., 2011]. This is based on quantitative measures of the strength of evidence for each hypothesis (Hi) rather than on "testing" null hypotheses based on test statistics and their associated P values. To quantify the strength of evidence for each hypothesis (Hi) – here the effect of each covariate on the breeding success- we used the common criteria AIC (the Akaike's Information Criteria), where AIC = - 2 log(L) + 2K [*Akaike,* 1973]. The term, -2 log(L), is the "deviance" of the model, with log(L) the maximized log-likelihood and K the total number of estimable parameters in the model. The chosen model is the one that minimizes the AIC, in orther words, minimizes the Kullback-Leibler distance between the model and truth. The ability of two models to describe the data was assumed to be "not different" if the difference in their AIC was < 2 [*Burnham and Anderson*, 2002]. Note the AIC is a way of selecting a model from a set of models based on information theory [*Burnham and Anderson*, 2002], and is largely used in biological sciences. While non-linear models may be more appropriate as ecological system relationships are likely more complex than linear relationships, without *a priori* knowledge of the mechanisms that could lead to such non-linear relationships, it is extremely difficult to set meaningful hypothesis to be included in the model selection.

Table 5 summarizes model selection. The model with the lowest AIC (highlighted in gray) suggests the BT pack ice as a sea ice covariate. If AIC are sorted from lowest to highest value, the next model includes the sea ice covariate MIZ calculated with the NASA algorithm. However, it shows a ΔAIC ~8 from the best model, and thus the NT MIZ is not well supported by the data in comparison to the best model. The relationship between BT pack ice and breeding success is negative [**Figure 11**]. In other words, a more extensive consolidated pack ice during winter tends to reduce breeding success the following summer by limiting foraging opportunities. The effect of the MIZ however was uncertain, contrary to what one may expect given the increased opportunities for foraging within the MIZ. However, if we had only used ice classifications based on the NASA Team algorithm, the model with the lowest AIC would have suggested an importance of the MIZ. We would have then concluded a negative effect of the MIZ on the breeding success of snow petrels, contrary to what one may expect given that the MIZ is the main feeding habitat of the species. By using both algorithms, we instead conclude that the breeding success of snow petrels is negatively affected by the pack ice area as calculated with the Bootstrap algorithm.

5. Discussion

While the main purpose for doing the classification of different ice categories is for interdisciplinary studies of sea bird breeding success, the results may also be useful for attribution of the observed sea ice changes. The positive trends in Antarctic sea ice extent are currently poorly understood and are at odds with climate model forecasts that suggest the sea ice should be declining in response to increasing greenhouse gases and stratospheric ozone depletion [e.g. *Turner et al*., 2013; *Bitz and Polvani*, 2012; *Sigmond and Fyfe*, 2010]. However, several modeling studies, such as those used in the phase 5 Coupled Model Intercomparison Project (CMIP5), have suggested that the sea ice increase over the last 36 years remains within the range of intrinsic of internal variability [e.g. *Bitz and Polvani*, 2012; *Turner et al*., 2013; *Mahlstein et al*., 2013; *Polvani and Smith,* 2013; *Swart and Fyfe*, 2013]. Earlier satellite from the 1960s and 1970s and from ship observations suggest periods of high and low sea ice extent, and thus high natural variability [*Meier et al.*, 2013; *Gallaher et al*., 2014]. Further evidence comes from ice core climate records, which suggest that the climate variability observed in the Antarctic during the last 50 years remains within the range of natural variability seen over the last several hundred to thousands of years [*Thomas et al*., 2013; *Steig et al*., 2013]. Thus, we may require much longer records to properly assess Antarctic sea ice trends in contrast to the Arctic, where negative trends are outside the range of natural variability and are consistent with those simulated from climate models.

While many assessments of how Antarctic sea ice trends and variability compare with climate models have focused on the net circumpolar sea ice extent, it is the regional variability that becomes more important. For example, *Hobbs et al*. [2015] argue that when viewing trends on a regional basis, the observed summer and autumn trends fall outside of the range of natural variability as simulated by present-day climate models, with the signal dominated by opposing trends in the Ross Sea and the Bellingshausen/Amundsen seas. These results have questioned the ability of climate models to correctly simulate processes at the regional level and within the southern ocean-atmosphere-sea ice coupled system.

The net take-away point from these studies is that the net circumpolar changes in sea ice extent do not enhance our understanding of how the Antarctic sea ice is changing. Instead our focus should be on what drives regional and seasonal sea ice changes, including feedbacks and competing mechanisms. The results of this study may help to better understand regional and total changes in Antarctic sea ice by focusing not only on the total ice area, but also on how the consolidated pack ice, the marginal ice zone and coastal polynyas are changing. Differences in climatologies and trends of the different ice classes may suggest different processes are likely contributing to their seasonal and interannual variability. In addition, the different contributions of ice categories towards the overall expansion of the Antarctic sea ice cover between algorithms may in turn influence attribution of the observed increase in SIE. For example, within the highly dynamic MIZ region, intense atmosphere-ice-ocean interactions take place [e.g. *Lubin and Massom*, 2006] and thus an expanding or shrinking MIZ may help to shed light on the relative importance of atmospheric or oceanic processes impacting the observed trends in total SIE. Another issue is whether or not new ice is forming along the outer edge of the pack ice or if it is all being dynamically transported from the interior.

However, a complication exists, what sea ice algorithm should be used for such assessments? In this study we focused on using passive microwave satellite data for defining the different ice categories used here as it is the longest time-series available and is not limited by polar darkness or clouds. However, results are highly dependent on which sea ice algorithm is used to look at the variability in these ice classes, which will also be important in assessing processes contributing to these changes as well as implications of these changes to the polar marine ecosystem. In this study, the positive trends in circumpolar sea ice extent over the satellite data record are primarily driven by statistically significant trends ($p<0.05$) in expansion of the consolidated pack ice in both sea ice algorithms. However, an exception occurs in the NASA Team sea ice algorithm after the ice pack reaches its seasonal maximum extent when the positive trends in the pack ice are no longer as large, nor statistically significant. Instead, positive trends in the MIZ dominate during September and October ($p<0.10$). This is in stark contrast to the Bootstrap algorithm, which shows a declining MIZ area from March through November.

The algorithms also give different proportions of how much the total ice cover consists of consolidated ice, MIZ or polynya area. In some regions, such as the Pacific Ocean sector, the NT algorithm suggests the MIZ is the dominant ice category whereas in the BT algorithm, the pack ice is dominant, which is true for all sectors analyzed in the Bootstrap algorithm. Considering the circumpolar ice cover, the MIZ in the NASA Team algorithm is on average twice as large as in the Bootstrap algorithm. In the Arctic, *Strong and Rigor* [2013] found the NASA Team algorithm gave about three times wider MIZ than the Bootstrap algorithm. In this case, the Bootstrap results agreed more with MIZ widths obtained from the National Ice Center (NIC).

While we find consistency in trends in pack ice and the MIZ, there are some important differences that may influence interpretation of processes governing sea ice changes. For example, in the Ross Sea, the largest regional positive trends in total SIE are found at a rate of 119,000 km^2 per decade [e.g. *Turner et al*., 2015], accounting for about 60% of the circumpolar ice extent increase. This is entirely a result of large positive trends in the pack ice in the BT algorithm from March to November ($p<0.01$) whereas the NT algorithm shows statistically significant increases in the MIZ. Several studies have suggested a link between sea ice anomalies in the Ross Sea and the wind-field associated with the Amundsen Sea Low (ASL) [e.g. *Fogt et al*., 2012; *Hosking et al*., 2013; *Turner et al*., 2012]. The strengthened southerly winds over the Ross Sea cause a more compacted and growing consolidated ice cover in the BT algorithm at the expense of a shrinking MIZ, whereas in the NT algorithm the area of the MIZ is increasing more than the pack ice during autumn, which may suggest a smaller sensitivity to thin ice growing in openings and leads for BT than for NT. While this is true as averaged over the entire Ross Sea sector, Figure 9 highlights that the area-averaged trends hide important spatial variability.

In the Weddell Sea, expansion of the overall ice cover is only statistically significant during the autumn months (MAM) [e.g. *Turner et al*., 2015]. During this time-period, both algorithms agree on statistically significant positive trends in the pack ice area, that extend through May for NT ($p<0.05$) and through June for BT ($p<0.05$). Statistically significant trends are also seen during March in the MIZ, with larger trends in the NT algorithm ($p<0.01$). Thus, overall expansion of sea ice in the Weddell during autumn is in part driven by expansion of the MIZ early in the season, after which it is controlled by further expansion of the consolidated pack.

In contrast, the B/A Sea is a region undergoing declines in the overall ice cover [e.g. *Parkinson and Cavalieri*, 2012; *Stammerjohn et al*., 2012]. Separating out trends for both the pack ice and the MIZ reveals positive trends during winter (JJA), and negative trends in the consolidated pack ice during the start of ice expansion in March and April. However, when averaging over the entire region, the trends are generally not statistically significant except for positive trends during winter in the NT algorithm. This is the only region where the BT algorithm does not show statistically significant trends in the pack ice. In the NT algorithm, the overall sea ice decline is largely a result of negative trends in the MIZ, consistent with the observation that the SIE trends in the Bellingshausen/Amundsen Sea are largely wind-driven, so it would be expected that the wind-driven compaction would lead to decreased MIZ and increased pack ice. In regards to potential coastal polynyas, the largest expansion of polynya area is found in the Bellingshausen/Amundsen Sea during November, whereas small increases in polynya area are found in both the Indian and Pacific sector during the ice expansion phase. Outside of these regions/months, no significant changes in coastal polynya area are observed.

Differences between the algorithms are not entirely surprising as the two algorithms use different channel combinations with different sensitivities to changes in physical temperature [*Comiso et al*., 1997; *Comiso and Steffen*, 2001]. In addition, the NT uses previously defined tie points for passive microwave radiances over known ice-free ocean, and ice types, defined as type A and B in the Antarctic, as the radiometric signature between first-year and multiyear ice in the Antarctic is lost. The ice is assumed to be snow-covered when selecting the tie points, which can result in an underestimation of sea ice concentration if the ice is not snow covered [e.g. *Cavalieri et al*., 1990]. While large-scale validation studies are generally lacking, a recent study of the interior of the ice pack in the Weddell Sea in winter suggested that the Bootstrap algorithm shows a better fit to upward looking sonar data [*Connolley*, 2005]. This suggests that broken water inside the pack ice as recorded by the NASA Team algorithm during winter may be erroneously detected.

However, another complication is that seasonal variations in sea ice and snow emissivity can be very large, leading to seasonal biases in either algorithm [e.g. *Andersen et al.*, 2007; *Willmes et al*., 2014; *Gloersen and Cavalieri*, 1986]. In addition, ice-snow interface flooding, formation of meteoric ice and snow metamorphism all impact sea ice concentrations, which have not been quantified yet for Antarctic sea ice, and trends in brightness temperatures found in the Weddell Sea may reflect increased melt rates or changes in the melt season [*Willmes et al.,* 2014]. The advantage of the Bootstrap algorithm is that the ice concentration can be derived without an *a priori* assumption about ice type, though consolidated ice data points are sometimes difficult to distinguish from mixtures of ice and open ocean due to the presence of snow cover, flooding or roughness effects.

While one may expect the Bootstrap algorithm to provide more accurate results than the NASA Team algorithm, near the coast the BT algorithm has been shown to have difficulties when temperatures are very cold. Because the NT algorithm uses brightness temperature ratios it is largely temperature independent. During summer or for warmer temperatures, the NT algorithm may indeed be biased towards lower sea ice concentrations whereas the BT algorithm may be biased towards higher ice concentrations [e.g. *Comiso et al.,* 1997]. This will result in different proportions of MIZ and consolidated pack ice. In the Arctic, the MIZ is not only driven by wave mechanics and flow breaking (dynamic origin), but also by melt pond processes in summer (thermodynamic origin) [*Arnsten et al*., 2015]. Thus, larger sensitivity of the NT algorithm to melt processes may be one reason for the larger discrepancy observed in the MIZ between the algorithms the Arctic. Interestingly, the BT algorithm shows less interannual variability in the MIZ, consolidated pack ice and potential coastal polynyas compared to NT (as shown by the smaller standard deviations). This would in turn influence assessments of atmospheric or oceanic conditions driving observed changes in the ice cover.

What is clear is that more validation is needed to assess the accuracy of these data products, especially for discriminating the consolidated pack ice from the MIZ. Errors likely are larger in the MIZ because of the coarse spatial resolution of the satellite sensors. The MIZ is very dynamic in space and time, making it challenging to provide precise delimitations using sea ice concentrations that are in turn sensitive to melt processes and surface conditions. Another concern is that mapping of the consolidated ice pack does not always mean a compact ice cover. The algorithms may indicate 100% sea ice concentration (e.g. a consolidated pack ice), when in reality the ice consists of mostly brash ice and small ice floes more representative of the MIZ. Future work will focus on validation with visible imagery.

Conclusions

Antarctic sea ice plays an important role in the polar marine ecosystem. While total Antarctic sea ice cover is expanding in response to atmospheric and oceanic variability that remains to be fully understood, one may expect that these increases would also be manifested in either equatorward progression of the MIZ or the consolidated pack ice or both, that in turn would impact the entire trophic web, from primary productivity, to top predator species, such as seabirds. In this study we identified several different ice categories using two different sets of passive microwave sea ice concentration data sets. The algorithms are in agreement as to the location of the northern edge of the total sea ice cover, but differ in regards to how much of the ice cover consists of the marginal ice zone, the consolidated ice pack, the size of potential polynyas as well as the amount of broken ice and open water within the consolidated ice pack. Here we use sea ice concentration thresholds of $0.15 \leq SIC < 0.80$ to define the width of the MIZ and $0.80 \leq SIC \leq 1.0$ to define the consolidated pack ice. Yet applying the same thresholds for both sea ice algorithms results in a MIZ from the NASA Team algorithm that is on average twice as large as in the Bootstrap algorithm and considerably more broken ice within the consolidated pack ice. Total potential coastal polynya areas ($SIC \leq 0.80$) also differ between the algorithms, though differences are generally smaller than for the MIZ and the consolidated pack ice. While we do not precisely resolve polynyas, these potential coastal polynyas (i.e. open water areas near the coast) are important foraging sites for sea birds.

While the spatial extents of the different ice classes may differ, the seasonal cycle is generally consistent between both algorithms. Climatologically, the advance of the consolidated ice pack happens over a much longer period (~7-8 months) than the retreat (~4-5 months), while the MIZ exhibits a longer advance period (~8-10 months). This seasonal cycle in expansion/contraction of the ice cover is in general agreement with results by *Stammerjohn et al.* [2008] who showed sea ice retreat begins in September at the outer most edge of the sea ice and continues poleward over the next several months. However, what these results show is that while the pack ice starts to retreat around September, this in turn results in a further expansion of the MIZ, the amount of which is highly dependent on which algorithm is used. The timing of when the maximum polynya extent is reached however can differ by several months between the algorithms in regions such as the Bellingshausen/Amundsen Sea and the Pacific Ocean.

Since the MIZ is an important region for phytoplankton biomass and productivity [e.g. *Park et al.,* 1999], mapping seasonal and interannual changes in the MIZ is important for understanding changes in top predator populations and distributions. However, as we show in this study, results are highly dependent on which sea ice algorithm is used for delineating the MIZ, which may result in different conclusions when using this data in ecosystem models. To hightlight this sensitivity, we examined the impact the winter MIZ and consolidated pack ice area as derived from both algorithms would have on the breeding success of snow petrels the following summer. The different proportions of MIZ and consolidated pack ice between algorithms affected the inferences made from models tested even if trends were of the same sign. Given the sensitivity of the relationships between the consolidated pack ice/MIZ and breeding success of this species, caution is warranted when doing this type of analysis as different relationships may emerge as a function of which sea ice data set is used in the analysis. Further work is needed to validate the accuracy of the distribution of the MIZ and consolidated pack ice from passive microwave so that the data will be more useful for future biological and ecosystem studies.

Acknowledgements

This work is funded under NASA Grant NNX14AH74G and NSF Grant PLR 1341548. We are grateful to Sharon Stammerjohn for her helpful comments on the manuscript. Gridded fields of the different ice classifications from both algorithms are available via ftp by contacting J. Stroeve. We thank all the wintering fieldworkers involved in the collection of snow petrel data at Dumont d'Urville since more than 50 years, as well as Institut Paul Emile Victor (program IPEV n°109, resp. H. Weimerskirch), Terres Australes et Antarctiques Françaises and Zone Atelier Antarctique (CNRS-INEE) for support.

References

Ainley, D.G., E. O'Connor, and R.J. Boekelheide. (1984). The marine ecology of birds in the Ross Sea, Antarctica, *Ornithological Monographs*, 32, 1-97.

Ainley, D. G., W.R. Fraser, C.W. Sullivan, J.J. Torres and T.L. Hopkins et al. (1986), Antarctic mesopelagic micronekton: Evidence from seabirds that pack ice affects community structure, *Science*, 232:847-849.

Ainley, D.G., Ribic, C. A., and Fraser, W. R. (1992). Does prey preference affect habitat choice in Antarctic seabirds? *Marine Ecology-Progress Series*, 90:207-221.

Ainley, D., J. Russell, S. Jenouvrier, E. Woehler, P. O. B. Lyver, W. R. Fraser, and G. L. Kooyman (2010), Antarctic penguin response to habitat change as Earth's troposphere reaches 2 C above preindustrial levels, *Ecological Monographs*, *80*(1), 49-66.

Akaike, H. (1973), Information theory as an extension of the maximum likelihood principle. In: Petrov BN, Csaki F (eds) Second international symposium on information theory. Akademiai Kiado, Budapest, pp 267–281.

Andersen, S., R. Tonboe, L. Kaleschke, G. Heygster and L.T. Pedersen, (2007), Intercomparison of passive microwave sea ice concentration retrievals over the high-concentration Arctic sea ice, *J. Geophys. Res*s., 112, C08004, doi:10.1029/2006JC003543.

Arnsten, A.E., A.J. Song, D.K. Perovich and J.A. Richter-Menge, (2015), Observations of the summer breakup of an Arctic sea ice cover, *Geophys. Res. Lett*., doi:10.1002/1015GL065224.

Arrigo, K. R., and G. L. van Dijken (2003), Phytoplankton dynamics within 37 Antarctic coastal polynya systems, *Journal of Geophysical Research: Oceans (1978–2012)*, *108*(C8).

Arrigo, K., G. L. van Dijken, and A. Strong (2015), Environmental controls of marine productivity hot spots around Antarctica, *J. Geophys. Res.-Oceans*, doi:10.1002/2015JC010888.

Atkinson, A., Siegel, V., Pakhomov, E., & Rothery, P. (2004). Long-term decline in krill stock and increase in salps within the Southern Ocean. *Nature*, doi:10.1038/nature02996.

Barbraud C., and O. Chastel, (1999), Early body condition and hatching success in the snow petrel Pagodroma nivea. *Polar Biol.,* 21:1-4.

Barbraud C. and H. Weimerskirch (2001), Contrasting effects of the extent of sea-ice on the breeding performance of an Antarctic top predator, the snow petrel Pagodroma nivea. *J. Avian Biol*., 32:297-302

Bintanja, R., G. J. Van Oldenborgh, S. S. Drijfhout, B. Wouters, and C. A. Katsman, (2013), Important role for ocean warming and increased ice-shelf melt in Antarctic sea-ice expansion, *Nat. Geosci*., 6, 376–379, doi:10.1038/ngeo1767.

Bitz, C.M. and L.M. Polvani, (2012), Antarctic climate response to stratospheric ozone depletion in a fine resolution ocean climate model, *Geophys. Res. Lett.,* doi:10.1029/2012GL053393.

Boyd PW, Jickells T, Law CS, Blain S, Boyle EA, et al. (2007). Mesoscale iron enrichment experiments 1993–2005: Synthesis and future directions. *Science* **315**: 612–617

Burnham, K. P., and D. R. Anderson. 2002. Model selection and multimodel inference : a practical information-theoretic approach. Springer, New York, ISBN:978-0-387-95364-9.

Burnham, K.P, D.R. Anderson and K.P. Huyvaert, (2011), AIC model selection and multimodel inference in behavioral ecology: some background, observations, and comparisons, *Behav. Ecol. Sociobiol.*, 65:23–35, doi:10.1007/s00265-010-1029-6.

Cavalieri, D. J., C. L. Parkinson, P. Gloersen, J. C. Comiso, and H. J. Zwally, (1999), Deriving Long-Term Time Series of Sea Ice Cover from Satellite Passive-Microwave Multisensor Data Sets, *J. Geophys. Res.*, 104, 15,803-15,814.

Cavalieri, D.J., B.A. Burns, and R.G. Onstott, (1990), Investigation of the effects of summer melt on the calculation of sea ice concentration using active and passive microwave data, *J. Geophys. Res*., 95, 5359-5369.

Chiswell, S. M. (2011), Annual cycles and spring blooms in phytoplankton: don't abandon Sverdrup completely, *Marine Ecology Progress Series*, *443*, 39-50.

Comiso, J. C., and F. Nishio. 2008. Trends in the Sea Ice Cover Using Enhanced and Compatible AMSR-E, SSM/I, and SMMR Data. *J. Geophys. Res.,* 113, C02S07, doi:10.1029/2007JC0043257.

Comiso, J. C., D. Cavalieri, C. Parkinson, and P. Gloersen (1997), Passive Microwave Algorithms for Sea Ice Concentrations: A Comparison of Two Techniques. *Rem. Sens. Environ*., 60(3):357-84.

Comiso, J.C. and K. Steffen (2001), Studies of Antarctic sea ice concentrations from satellite data and their applications, *J. Geophys. Res*., 106(C12):31361-31385.

Delord, K., C. Barbraud, C.A. Bost, Y. Cherel, C. Guinet, and H. Weimerskirch. 2013. Atlas of top predators from French Southern Territories in the Southern Indian Ocean. CEBC-CNRS. pp. 252.

Ferrari, R., S. T. Merrifield, and J. R. Taylor (2014), Shutdown of convection triggers increase of surface chlorophyll, *J. Marine Systems*, doi:10.1016/j.jmarsys.2014.02.009.

Flores, H., J. Andries van Franeker, V. Siegel, M. Haraldsson, V. Strass, E.H. Meesters, U. Bathmann, and W.-J. Wolff, (2012), The Association of Antarctic Krill Euphausia superba with the Under-Ice Habitat, *Plos One*, doi:101371/journal.pone.0031775.

Fogt RL, Wovrosh AJ, Langen RA, Simmonds I (2012) The characteristic variability and connection to the underlying synoptic activity of the Amundsen–Bellingshausen Seas low, *J Geophys Res.* doi:10.1029/2011JD017337

Gallaher, D., G. G. Campbell, and W. N. Meier (2014), Anomalous variability in Antarctic sea ice extents during the 1960s with the use of Nimbus data. *IEEE J. Selected Topics in Appl. Earth Obs. And Rem. Sens*., 7(3), 881-887, doi:10.1109/JSTARS.2013.2264391.

Gloersen, P., W. J. Campbell, D. J. Cavalieri, J. C. Comiso, C. L. Parkinson, H. J. Zwally, "Arctic and Antarctic Sea Ice, 1978-1987L Satellite Passive Microwave Observations and Analysis," *NASA Spec. Publ.,* Vol. 511, 290 pp, 1992.

Gloersen, P. and D.J. Cavalieri, (1986), Reduction of weather effects in the calculation of sea ice concentration from microwave radiances, *J. Geophys. Res*., 91, 3913-3919.

Hobbs, W.R, N.L. Bindoff, N. L. and M.N. Raphael, (2015), New perspectives on observed and simulated Antarctic Sea ice extent trends using optimal fingerprinting techniques, *J. Clim.* **28**,1543–1560, doi:10.1175/JCLI-D-14-00367.1.

Hobbs, W.R. and M.N. Raphael (2010), The Pacific zonal asymmetry and its influence on Southern Hemisphere sea ice variability. *Antarctic Science*, 22 (05), 559-571, doi: 10.1017/S0954102010000283.

Holland, P. and R. Kwok (2012), Wind-driven trends in Antarctic sea-ice drift, *Nature Geoscience*, 5, 872-875, doi:10.1038/ngeo1627.

Hosking JS, Orr A, Marshall GJ, Turner J, Phillips T (2013) The influence of the Amundsen–Bellingshausen Seas low on the climate of West Antarctica and its representation in coupled climate model simulations. *J Clim*., 26:6633–6648

Ivanova, N., and others, (2015), Satellite passive microwave measurements of sea ice concentration: an optimal algorithm and challenges, *The Cryosphere Discuss*., 9, doi:10.5194/tcd-9-1269-2015.

Ivanova, N., O.M. Johannessen, L. Toudal Pederson and R.T. Tomboe (2014), Retrieval of Arctic sea ice parameters by satellite passive microwave sensors: A comparison of eleven sea ice concentration algorithms, *IEEE Trans. Geos. Rem. Sens*., 52(11), doi:10.1109/TGRS.2014.2301136.

Jaiser, R., K. Dethloff, D. Handor, A. Rinke and J. Cohen, (2012), Impact of sea ice cover changes on the Northern Hemisphere atmospheric winter circulation, *Tellus*, 64, 11595, doi:10.3402/tellusa.v64i0.11595.

Jenouvrier, S., C Barbraud, and H. Weimerskirch, (2005), Long-Term Contrasted Reponses to climate of two Antarctic seabird species, *Ecology* 86:2889–2903. http://dx.doi.org/10.1890/05-0514

Kohout, A.L, M.J.M. Williams, S.M. Dean and M.H. Meylan, (2014), Storm-induced sea-ice breakup and the implications for ice extent, Nature, 509, 604-608, doi:10.1038/nature13262..

Li, Y., R. Ji, S. Jenouvrier, M. Jin and J. Stroeve (2016), Synchronicity between ice retreat and phytoplankton bloom in circum-Antarctic polynyas, *Geophys. Res. Lett.*, doi://10.1002/2016GL067937.

Loeb, V. J., V. Siegel, O. Holm-Hansen, R. Hewitt, W. Fraser, W. Trivelpiece, and S. G. Trivelpiece, (1997), Effects of sea- ice extent and krill or salp dominance on the Antarctic food web*, Nature* **387**:897–900.

Lubin, D. and R. Massom (2006), Sea ice. In Polar remote sensing volume i: atmosphere and oceans, Springer, Berlin, pp 309-728.

Mahlstein, I. P.R. Gent and S. Solomon, (2013), Historical Antarctic mean sea ice area, sea ice trends, and winds in CMIP5 simulations, *J. Geophys. Res. Atmos*., doi:10.1002/jgrd.50443.

Maksym, T.E. E. Stammerjohn, S. Ackley and R. Massom (2012), Antarctic sea ice – A polar opposite? Oceanography, 25, 140-151, doi:10.5670/oceanog.2012.88.

Meier, W., D. Gallaher, and G. G. Campbell (2013), New estimates of Arctic and Antarctic sea ice extent during September 1964 from recovered Nimbus I satellite imagery, The Cryosphere 7, 699-705, doi:10.5194/tc-7-699-2013.

Meier, W., F. Fetterer, M. Savoie, S. Mallory, R. Duerr, and J. Stroeve, (2013), updated 2015. *NOAA/NSIDC Climate Data Record of Passive Microwave Sea Ice Concentration, Version 2*. Boulder, Colorado USA: National Snow and Ice Data Center, http://dx.doi.org/10.7265/N55M63M1

Morales-Maqueda, M.A., A.J. Willmott, and N.R.T. Biggs (2004), Polynya dynamics: a review of observations and modelling, Reviews of Geophysics, 24, doi:10.1029/2002RG000116.

Olivier, F., Franeker, J. A. V., Creuwels, J. C. S., & Woehler, E. J. (2005), Variations of snow petrel breeding success in relation to sea-ice extent: detecting local response to large-scale processes? *Polar Biology*, *28*(9), 687–699. http://doi.org/10.1007/s00300-005-0734-5

Park, M. K., S.R. Yang, S.H. Kang, K.H. Chung, and J.H. Shim, (1999), Phytoplankton biomass and primary production in the marginal ice zone of the northwestern Weddell Sea during austral summer, *Polar Biol., 21*, *251*–261.

Parkinson, C. L. and D.J. Cavalieri, (2012). Antarctic Sea Ice Variability and Trends, 1979–2010. *The Cryosphere,* 6:871-880. doi:10.5194/tcd-6-931-2012.

Piatt, I., & Sydeman, W. (2007), Seabirds as indicators of marine ecosystems. *Marine Ecology Progress Series*, *352*, 199–204. http://doi.org/10.3354/meps07070.

Polvani, L.M. and K.L. Smith, (2013), Can natural variability explain observed Antarctic sea ice trends? New modeling evidence from CMIP5, Geophys. Res. Lett., 40(12), 3195-3199, doi:10.1002/grl.50578.

Raphael, M.N. and W. Hobbs (2014), The influence of the large-scale atmospheric circulation on Antarctic sea ice during ice advance and retreat seasons, *Geophys. Res. Lett*., doi:10.1002/2014GL060365.

Rayner, N.A., D.E. Parker, E.B. Horton, C.K. Folland, L.V. Alexander, D.P. Rowell, E.C. kent, and A. Kaplan, (2003), Global analyses of sea surface temperature, sea ice, and night marine air temperature since the late nineteenth century, *J. Geophys. Res*., 118, doi:10.1029/2002JD002670.

Reid, P., S. Stammerjohn, R. Massom, T. Scambos, and J. Leiser (2015), The record 2013 Southern Hemisphere sea-ice extent maximum. *Ann. Glaciology*, 56(69), pp. 99-106(8).

Serreze, M.C. and J.C. Stroeve, (2015), Arctic Sea Ice Trends, Variability and Implications for Seasonal Ice Forecasting, *Phil. Trans. A.,* 373, 20140159, doi:10.1098/rsta.2014.0159.

Simmonds, I. (2015), Comparing and contrasting the behavior of Arctic and Antarctic sea ice over the 35 year period 1979-2013, *Annals of Glaciology*, 56(69), 18-28.

Smith Jr, W. O., and D. Barber (2007), *Polynyas: Windows to the World: Windows to the World*, Elsevier.

Smith, R.C. and S.E. Stammerjohn, (2001), Variations of surface air temperature and sea ice extent in the Western Antarctic Peninsula (WAP) region, *Annals of Glaciology* 33, 493–500.

Stammerjohn, S.E., D.G. Martinson, R.C. Smith, X. Yuan and D. Rind, (2008), Trends in Antarctic annual sea ice retreat and advance and their relation to El Nino-Southern Oscillation and Southern Annular Mode variability, *J. Geophys. Res.,* 108, C03S90, doi:10.1029/2007JC004269.

Stammerjohn, S., R. Massom, D. Rind, and D. Martinson, 2012: Regions of rapid sea ice change: An inter-hemispheric seasonal comparison. *Geophys. Res. Lett.*, **39**, L06501, doi:10.1029/2012GL050874.

Sigmond, M. and J.C. Fyfe, (2010), Has the ozone hole contributed to increased Antarctic sea ice extent?, *Geophys. Res. Lett*., 37, L18502, doi:1029/2010GL044301.

Steig, E. J., et al. (2013), Recent climate and ice-sheet changes in West Antarctica compared with the past 2,000 years, *Nat. Geosci.*, **6**, 372–375.

Stroeve, J.C., M.C. Serreze, J.E. Kay, M.M. Holland, W.N. Meier and A.P. Barrett (2012), The Arctic's rapidly shrinking sea ice cover: A research synthesis, *Clim. Change*, doi: 10.1007/s10584-011-0101-1.

Strong, C. and I.G. Rigor, (2013), Arctic marginal ice zone trending wider in summer and narrower in winter, *Geophys. Res. Lett*., 40, doi:10.1002/grl.50928.

Swart, N.C. and J.C. Fyfe, (2013), The influence of recent Antarctic ice sheet retreat on simulated sea ice area trends, *Geophys. Res. Lett*., doi:1002/grl.50820.

Thomas, E.R., T.J. Bracegirdle, J. Turner and E.W. Wolff, (2013), A 308 year record of climate variability in West Antarctica, *Geophys. Res. Lett*., doi:10.1002/2013GL057782.

Turner J, T. Phillips, S. Hosking, G.T. Marshall and A. Orr, (2012) The Amundsen Sea Low, *Int J. Climatol*., 33:1818–1829.

Turner J., J. S. Hosking, T. Phillips, and G. J. Marshall, (2013), Temporal and spatial evolution of the Antarctic sea ice prior to the September 2012 record maximum extent. *Geophys. Res. Lett*., 40, 5894–5898, doi: 10.1002/2013GL058371.

Turner, J., J.S. Hosking, G.J. Marshall, T. Phillips, T.J. Bracegirdle, (2015), Antarctic sea ice increase consistent with intrinsic variability of the Amundsen Sea Low, *Clim. Dyn*., doi:10.1007/s00382-015-2709-9.

Wadhams, P., (1986), The seasonal ice zone, The Geophysics of Sea Ice, NATO ASI Series, 825–991, doi:10.1007/978-1-4899-5352-0_15.

Watkins, A.B. and I. Simmonds, (1999), A late spring surge in open water of the Antarctic sea ice pack, *Geophys. Res. Lett*., 26, doi:10.1029/1999GL900292.

Willmes, S., M. Nicolaus and C. Haas, (2014), the microwave emissivity variability of snow covered first-year sea ice from late winter to early summer: a model study, *The Cryosphere*, 8, 891-904, doi:10.5194/tc-8-891-2014.

Yun, L., R. Ji, S. Jenouvrier, M. Jin and J. Stroeve, (2015), Synchronicity between ice retreat and phytoplankton bloom in circum-Antarctic Polynyas, *Geophys. Res. Lett*., 43(5), 2086-2093, doi:10.1002/2016GL067937.

Tables

Table 1. Sea ice categories defined in this study.

Region	Definition	Binary Classification Value
Outer MIZ	Outer region of sea ice with ice concentration between 15% and 80%	16
Inner Polynya	Region near the coast with concentration < 80% south of 80% concentration	32
Distant ice	Scattered sea ice regions north of MIZ, possibly islands or atmospheric storms	48
Pack Ice	Ice concentration > 80%	80
Inner open water	Concentration < 15% south of MIZ	112
Open pack ice	Concentration > 15% and < 80% within consolidated ice region	128

Table 2. Monthly mean extents of the different ice classes. Values are only listed for the consolidated pack ice, the marginal ice zone and the potential coastal polynya area. Values are listed in 10^6 km^2.

	NASA Team			Bootstrap		
Total Antarctic						
Month	**MIZ**	**Polynya**	**Pack Ice**	**MIZ**	**Polynya**	**Pack Ice**
January	2.44	0.31	1.94	2.06	0.36	2.27
February	1.51	0.20	1.18	1.25	0.22	1.49
March	2.03	0.25	1.42	1.65	0.24	2.08
April	2.71	0.42	3.27	1.84	0.31	4.62
May	3.07	0.62	5.85	1.97	0.37	7.79
June	3.63	0.69	8.22	2.31	0.37	10.65
July	4.03	0.66	10.31	2.53	0.35	13.00
August	4.75	0.62	11.29	2.88	0.34	14.49
September	5.41	0.63	11.31	3.19	0.35	14.89
October	5.41	0.74	10.83	3.39	0.38	14.16
November	5.62	1.02	7.92	3.69	0.63	11.10
December	5.05	0.88	3.81	3.56	0.81	5.43
Annual	3.83	0.59	6.49	2.54	0.39	8.53
Ross Sea						
Month	**MIZ**	**Polynya**	**Pack Ice**	**MIZ**	**Polynya**	**Pack Ice**
January	0.83	0.10	0.28	0.68	0.13	0.40
February	0.47	0.05	0.11	0.40	0.07	0.19
March	0.62	0.10	0.34	0.45	0.09	0.57
April	0.60	0.15	1.22	0.37	0.09	1.63
May	0.60	0.15	1.93	0.36	0.08	2.43
June	0.67	0.15	2.29	0.40	0.08	2.91
July	0.75	0.14	2.63	0.44	0.07	3.27
August	0.91	0.12	2.67	0.50	0.07	3.43
September	0.98	0.13	2.64	0.54	0.08	3.46
October	0.86	0.17	2.73	0.55	0.09	3.39
November	0.89	0.30	2.19	0.59	0.17	2.87
December	1.17	0.32	0.92	0.76	0.26	1.45
Annual	0.78	0.16	1.67	0.50	0.11	2.18
Bellinghausen/Amundsen Sea						
Month	**MIZ**	**Polynya**	**Pack Ice**	**MIZ**	**Polynya**	**Pack Ice**
January	0.35	0.07	0.32	0.29	0.08	0.38
February	0.28	0.05	0.16	0.22	0.06	0.21
March	0.37	0.06	0.10	0.27	0.07	0.21
April	0.50	0.07	0.20	0.29	0.06	0.48
May	0.54	0.12	0.42	0.31	0.06	0.83
June	0.63	0.16	0.66	0.37	0.05	1.17
July	0.68	0.17	0.89	0.43	0.05	1.45
August	0.79	0.15	1.01	0.51	0.05	1.60
September	0.84	0.14	1.00	0.51	0.05	1.62
October	0.73	0.14	0.97	0.46	0.06	1.50
November	0.69	0.13	0.86	0.45	0.08	1.25
December	0.57	0.11	0.55	0.42	0.11	0.72
Annual	0.58	0.12	0.60	0.38	0.06	0.96
Weddell Sea						
Month	**MIZ**	**Polynya**	**Pack Ice**	**MIZ**	**Polynya**	**Pack Ice**
January	0.72	0.12	0.93	0.60	0.11	1.07
February	0.37	0.08	0.70	0.30	0.06	0.84
March	0.47	0.06	0.87	0.38	0.04	1.07
April	0.69	0.07	1.49	0.46	0.05	1.87
May	0.82	0.10	2.53	0.54	0.06	3.04
June	0.96	0.10	3.62	0.64	0.06	4.21
July	1.08	0.08	4.51	0.65	0.05	5.16

August	1.39	0.08	4.73	0.75	0.06	5.62
September	1.62	0.09	4.67	0.83	0.06	5.78
October	1.51	0.13	4.42	0.84	0.07	5.48
November	1.53	0.31	3.34	0.86	0.14	4.56
December	1.87	0.33	1.65	1.24	0.30	2.33
Annual	1.09	0.13	2.80	0.67	0.09	3.43
Indian Ocean						
Month	**MIZ**	**Polynya**	**Pack Ice**	**MIZ**	**Polynya**	**Pack Ice**
January	0.26	0.01	0.16	0.23	0.02	0.18
February	0.15	0.01	0.06	0.14	0.01	0.08
March	0.24	0.01	0.03	0.24	0.02	0.06
April	0.43	0.01	0.16	0.35	0.05	0.30
May	0.57	0.13	0.55	0.43	0.08	0.80
June	0.75	0.14	1.04	0.53	0.08	1.40
July	0.82	0.13	0.59	0.54	0.07	2.05
August	0.87	0.11	2.09	0.57	0.06	2.59
September	1.03	0.12	2.24	0.67	0.07	2.81
October	1.33	0.15	2.02	0.87	0.08	2.71
November	1.62	0.18	1.10	1.13	0.13	1.75
December	0.94	0.07	0.37	0.74	0.09	0.55
Annual	0.75	0.10	0.96	0.54	0.06	1.29
Pacific Ocean						
Month	**MIZ**	**Polynya**	**Pack Ice**	**MIZ**	**Polynya**	**Pack Ice**
January	0.28	0.01	0.24	0.25	0.02	0.26
February	0.23	0.01	0.14	0.19	0.02	0.17
March	0.34	0.02	0.10	0.31	0.03	0.15
April	0.51	0.05	0.20	0.38	0.06	0.34
May	0.54	0.11	0.43	0.35	0.10	0.67
June	0.61	0.14	0.62	0.38	0.11	0.93
July	0.70	0.14	0.73	0.45	0.10	1.10
August	0.81	0.14	0.79	0.54	0.09	1.19
September	0.93	0.14	0.76	0.63	0.10	1.17
October	0.96	0.14	0.71	0.68	0.09	1.08
November	0.88	0.10	0.44	0.66	0.11	0.70
December	0.49	0.05	0.30	0.41	0.06	0.38
Annual	0.61	0.09	0.46	0.44	0.07	0.69

Table 3. Comparison of trends in the marginal ice zone, polynyas and the consolidated pack ice for March through November (1979 to 2013) for both the NASA Team and Bootstrap sea ice algorithms. Trends are computed in km^2 per year. Statistical significance at the 90th, 95th and 99th percentiles are denoted by $^{+}$, $^{++}$ and $^{+++}$, respectively. Results are only shown for March through November.

	NASA Team			Bootstrap		
Total Antarctic						
Month	**dMIZ/dt**	**dPoly/dt**	**dPack/dt**	**dMIZ/dt**	**dPoly/dt**	**dPack/dt**
March	+2,900	+700	+14,300^{+++}	+4,900	-300	+18,000^{+++}
April	-8,200	-500	+29,600^{+++}	-10,400	-1000	+38,000^{+++}
May	-9,400	-2,400	+35,000^{+++}	-8,500	-2,200	+41,300^{+++}
June	-10,100	-5,100	+32,900^{+++}	-9,200	-2,400	+52,400^{+++}
July	-3,400	-5,700	+22,600^{++}	-6,600	-2,300	+25,200^{+++}
August	+3,700	-3,600	+11,900	-6,200	-1,500	+31,800^{+++}
September	+10,900^{+}	-3,300	+3,700	-4,200	-1,400	+39,400^{+++}
October	+9,600^{+}	-4,900	+7,300	-4,300	-2,900	+25,200^{+++}
November	+2,600	-4,000	+6,000	-9,800	-3,700	+29,400^{+++}
Ross Sea						
Month	**dMIZ/dt**	**dPoly/dt**	**dPack/dt**	**dMIZ/dt**	**dPoly/dt**	**dPack/dt**
March	+2,800	+300	+4,100	+1,500	-100	+7,700^{++}
April	-1,400	-1,500	+12,400^{++}	-2,700	-1,400	+14,600^{+++}
May	+2,600^{+}	-2,200	+11,100^{++}	-700	-1,100	+16,400^{+++}
June	0	-1,200	+12,700^{++}	-2,000	-800	+18,600^{+++}
July	+700	-700	+8,200^{+}	-700	-600	+14,200^{+++}
August	+6,900^{+++}	-1,600	+3,400	+500	-900	+12.700^{+++}
September	+4,800^{++}	-1,200	+1,800	-700	-700	+15,100^{+++}
October	+5,400^{+++}	-2,300	+7,300^{+}	+1,100	-1,300	+17,600^{+++}
November	+3,700^{+}	-1,200	+4,400	-700	-1,600	+13,700^{+++}
Bellinghausen/Amundsen Sea						
Month	**dMIZ/dt**	**dPoly/dt**	**dPack/dt**	**dMIZ/dt**	**dPoly/dt**	**dPack/dt**
March	-7,500	-1,500	-2,800	-2,400	-1,700	-7,500
April	-8,600	-800	-3,100	-3,100	-900	-7,700
May	-8,600	-1,200	+2,800	-2,100	-800	-4,600
June	-6,800	-2,600	+8,500^{+++}	-2,100	-500	+1,300
July	-3,500	-2,500	+10,100^{+++}	-700	-700	+4,000
August	-1,200	-700	+7,000^{+}	+500	-200	+2,700
September	+2,600	-500	-300	+1,500^{+}	-200	-100
October	-800	-200	-1,100	-300	-200	-1,800
November	+2,600	+1,000^{++}	-1,400	+1,600	+600^{+}	+300
Weddell Sea						
Month	**dMIZ/dt**	**dPoly/dt**	**dPack/dt**	**dMIZ/dt**	**dPoly/dt**	**dPack/dt**
March	+4,100^{++}	+1,300^{++}	+9,500^{++}	+2,600^{++}	+600^{+}	+13,600^{+++}
April	+1,700	+400	+12,000^{++}	-2,000	+200	+19,200^{+++}
May	-100	-400	+9,400^{++}	-1,500	-600	+14,400^{+++}
June	-2,300	-900	+100	-4,800	-600	+8,800^{++}
July	-2,900	-1,100	-4,800	-4,200	-400	-100
August	-1,700	-700	-5,100	-3,500	-100	+600
September	-200	-600	-100	-2,900	-200	+4,900
October	+4,300	-1,400	-8,800	-3,700	-700	+3,400
November	-2,100	-3,500	-4,700	-6,300	-2,200	+700
Indian Ocean						
Month	**dMIZ/dt**	**dPoly/dt**	**dPack/dt**	**dMIZ/dt**	**dPoly/dt**	**dPack/dt**
March	+2,500^{++}	+300^{+}	+9,500^{++}	+2,100^{++}	+300^{+}	+1,500^{++}
April	+1,500^{+}	+600^{+}	+12,000^{++}	-500	+300	+5,200^{+++}
May	-200	+600^{+}	+9,400^{++}	-1,400	+100	+7,700^{+++}
June	+2,600^{+}	-500	+100	+900	-300	+7,600^{++}
July	+3,500^{+}	-700	-4,800	+100	-100	+7,600^{++}
August	+1,300	-300	-5,100	-1,500	0	+9,900^{+++}

September	+4,600^{+}	-900	-100	+400	-100	+6,700^{++}
October	+1,900	-900	-8,800	-200	-400	+8,600^{++}
November	+2,000	-200	-4,700	-500	-400	+8,700^{++}
			Pacific Ocean			
Month	**dMIZ/dt**	**dPoly/dt**	**dPack/dt**	**dMIZ/dt**	**dPoly/dt**	**dPack/dt**
March	+1,100	+400^{+++}	+2,800^{+++}	+1,100^{++}	+600^{+++}	+1,500^{++}
April	-1,400	+800^{+++}	+5,600^{+++}	-2,100	+700^{+++}	+5,200^{+++}
May	-3,000	+800^{++}	+6,100^{+++}	-2,800	+300^{+}	+7,700^{+++}
June	-3,600	+200	+7,000^{+++}	-1,200	-300	+7,600^{++}
July	-1,300	-700	+5,700^{++}	-100	-400	+7,600^{++}
August	-1,500	-300	+2,200	-2,200	-300	+9,900^{+++}
September	-900	-100	+1,400	-2,500	-300	+6,700^{++}
October	-1,200	0	+3,700^{++}	-1,100	-300	+8,600^{++}
November	-3,500	-500	+4,400^{++}	-4,000	-200	+8,700^{++}

Table 4. Monthly latitude/longitude corners used for assessment of sea ice conditions on snow petrel breeding success. These areas were defined from the distribution of snow petrels recorded from miniaturized saltwater immersion geolocators during winter [*Delord et al*., 2016].

	April	**May**	**June**	**July**	**August**	**September**
$Latitude_1$	-65	-65	-65	-65	-65	-65
$Latitude_2$	-60	-60	-60	-60	-55	-55
$Longitude_1$	90	65	50	35	25	50
$Longitude_2$	120	120	120	120	115	140

Table 5. Results of model selection for the relationship between pack ice and MIZ on breeding success of snow petrel. The model with the lowest AIC is highlighted in gray. AIC scores are often interpreted as difference between the best model (smallest AIC) and each model referred as ΔAIC. According to information theory, models with $\Delta AIC < 2$ are both likely [*Burnham and Anderson*, 2002] but if a model shows a $\Delta AIC > 4$ it is unlikely in comparison with the best model (smallest AIC).

Model	**Variable**	**AIC**	**Slope**
Bootstrap	MIZ	931.86	-0.57544
NASA Team	MIZ	887.11	-1.31416
Bootstrap	Pack ice	879.17	-1.04223
NASA Team	Pack ice	927.8	-0.41916

List of Figures

Figure 1. Example of a radial profile from 50 to 90S at -11.60 degrees West on 3 September 1990, showing the different sea ice classifications found along this transect.

Figure 2: Samples of ice classification on day 70 (March) and day 273 (September) 2013. Results are shown for both the NASA Team (top) and Bootstrap (bottom) sea ice algorithms. The MIZ (red) represents regions of sea ice concentration between 15 and 80% from the outer ice edge, the pack ice is shown in light purple, representing regions of greater than 80% sea ice concentration. Orange regions within the pack ice represent coherent regions of less than 80% sea ice concentration, pink areas open water and green regions of less than 80% sea ice concentration near the Antarctic coastline. Dark blue represents the ocean mask applied to remove spurious ice concentrations beyond the ice edge.

Figure 3. Southern hemisphere regions as defined by *Parkinson and Cavalieri* [2012].

Figure 4. Location of the mean 1981-2010 outer marginal ice edge for both the NASA Team and Bootstrap algorithms.

Figure 5. Long-term (1979-2014) and standard deviation (shading) of the seasonal cycle in total Antarctic extent of the consolidated pack ice, the outer marginal ice zone, polynyas, open pack ice (or broken ice within the pack ice), and inner open water. There are essentially no scattered ice floes outside of the MIZ. NASA Team results are shown on the left and the Bootstrap on the right.

Figure 6. Long-term (1979-2014) seasonal cycle in regional sea ice extent of the consolidated pack ice, the outer marginal ice zone, polynyas, open pack ice (or broken ice within the pack ice), and inner open water. Results for the NASA Team algorithm are shown on the left and Bootstrap on the right, and for the Ross, Bellingshausen/Amundsen, Weddell, Indian and Pacific Oceans.

Figure 7. Expansion (red) or contraction (blue) of the outer ice edge (top), the width of the marginal ice zone (middle) and the width of the pack ice from 1979 to 2014 during the month of September relative to 60S.

Figure 8. Daily trends (1979 to 2014) in the consolidated pack ice, the outer MIZ and potential coastal polynyas for the entire Antarctic sea ice cover for the NASA Team (left) and Bootstrap (right) algorithms. Trends are provided in 10^6 km^2 a^{-1}.

Figure 9. Daily (1979-2014) trends in regional sea ice extent of the consolidated pack ice (top) and the outer marginal ice zone (bottom). Results for the NASA Team algorithm (left) and Bootstrap (right) are shown as a function of longitude. Trends are provided in 10^6 km^2 a^{-1}. Note the difference in color bar scales. Regions not statistically significant are highlighted.

Figure 10. Time-series of seasonal mean MAM (top), JJA (middle) and SON (bottom) marginal ice zone (left) and consolidated pack ice (right) for both sea ice algorithms; NASA Team is shown in red, Bootstrap in black. Shading represents one standard deviation. Note the difference in y-axis between the pack ice and the MIZ plots.

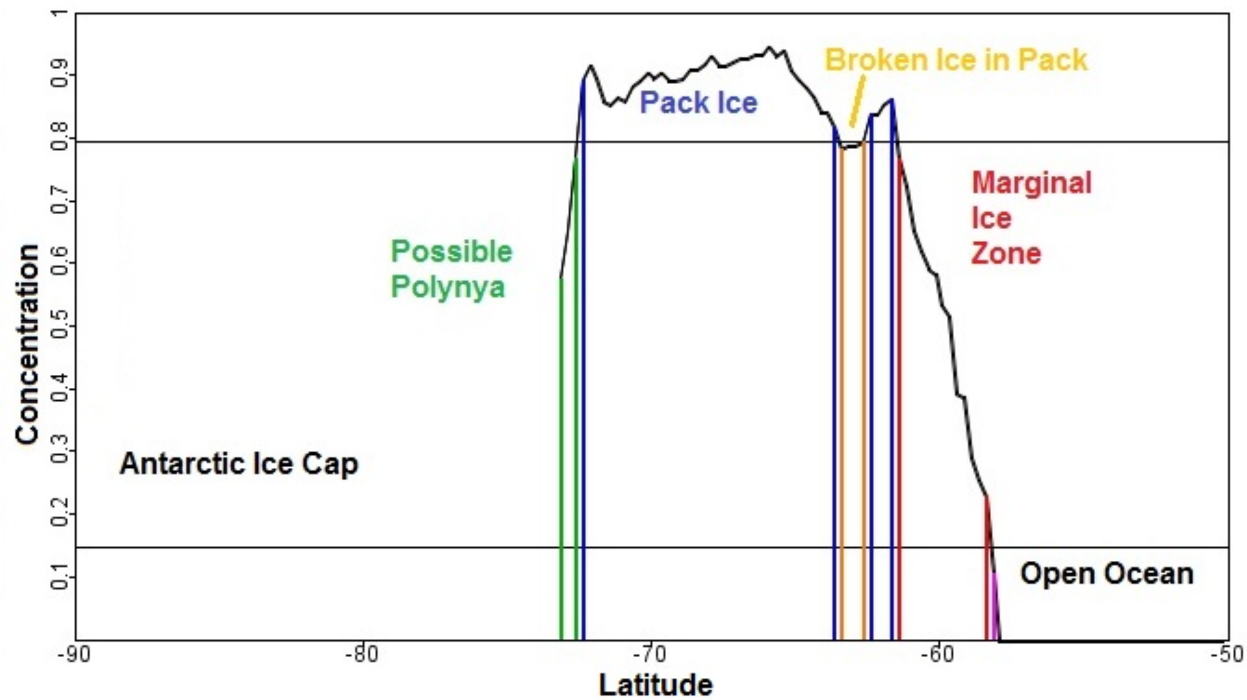

Figure 1. Example of a radial profile from 50 to 90S at -11.60 degrees West on 3 September 1990, showing the different sea ice classifications found along this transect.

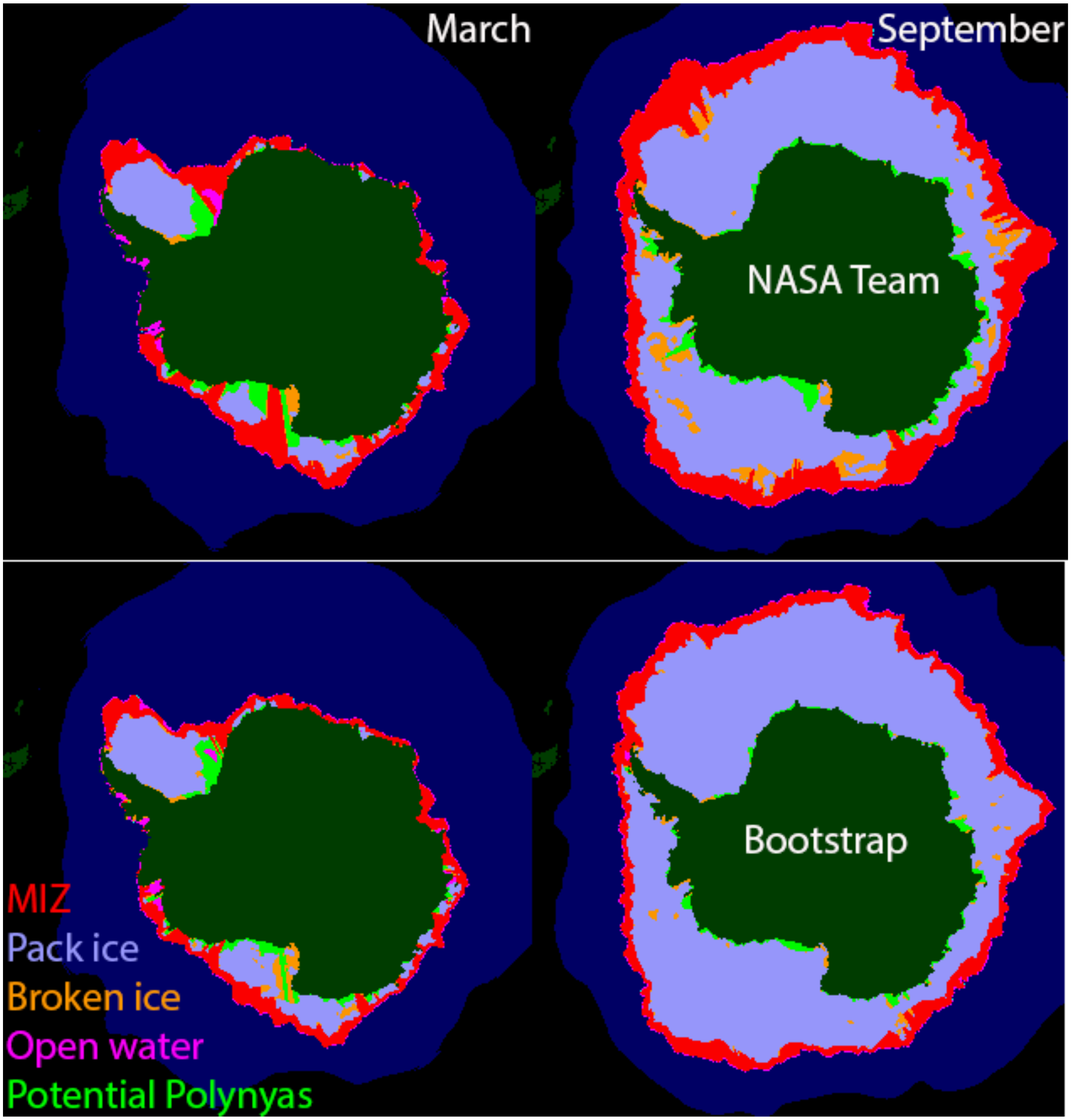

Figure 2: Samples of ice classification on day 70 (March) and day 273 (September) 2013. Results are shown for both the NASA Team (top) and Bootstrap (bottom) sea ice algorithms. The MIZ (red) represents regions of sea ice concentration between 15 and 80% from the outer ice edge, the pack ice is shown in light purple, representing regions of greater than 80% sea ice concentration. Orange regions within the pack ice represent coherent regions of less than 80% sea ice concentration, pink areas open water and green regions of less than 80% sea ice concentration near the Antarctic coastline. Dark blue represents the ocean mask applied to remove spurious ice concentrations beyond the ice edge.

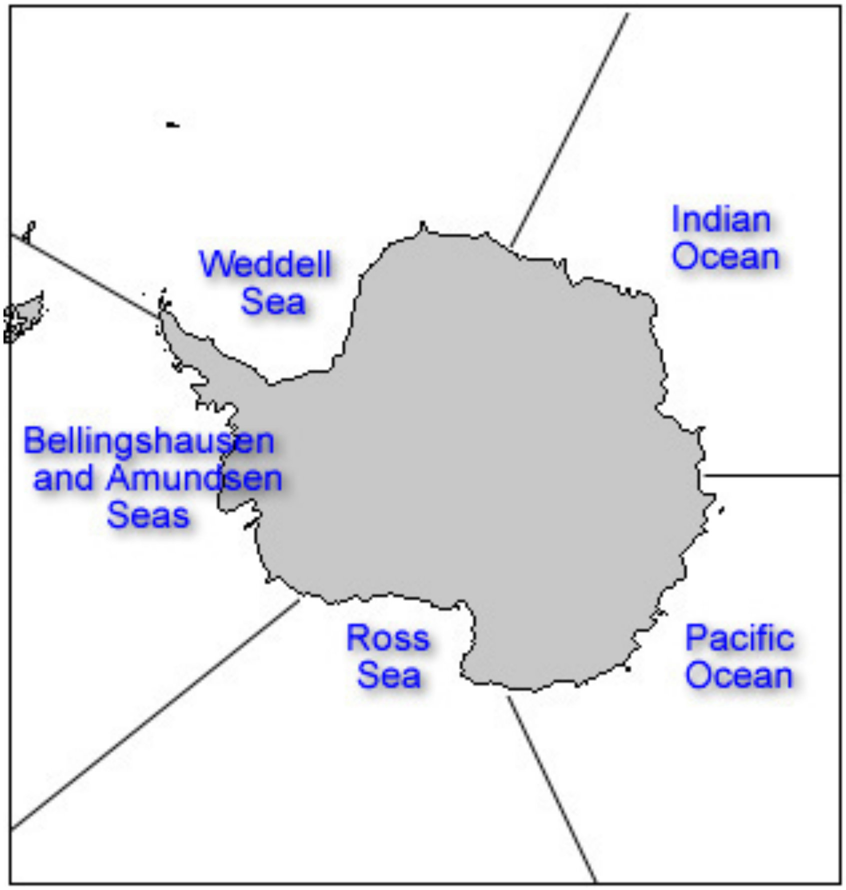

Figure 3. Southern hemisphere regions as defined by *Parkinson and Cavalieri* [2012].

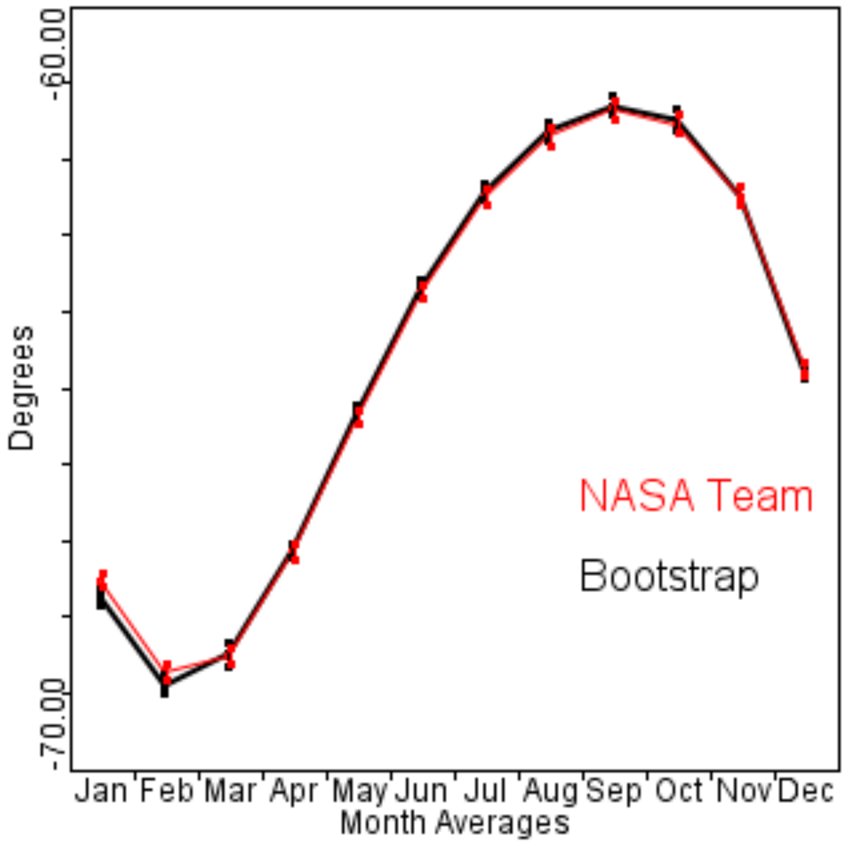

Figure 4. Location of the mean 1981-2010 outer marginal ice edge for both the NASA Team and Bootstrap algorithms.

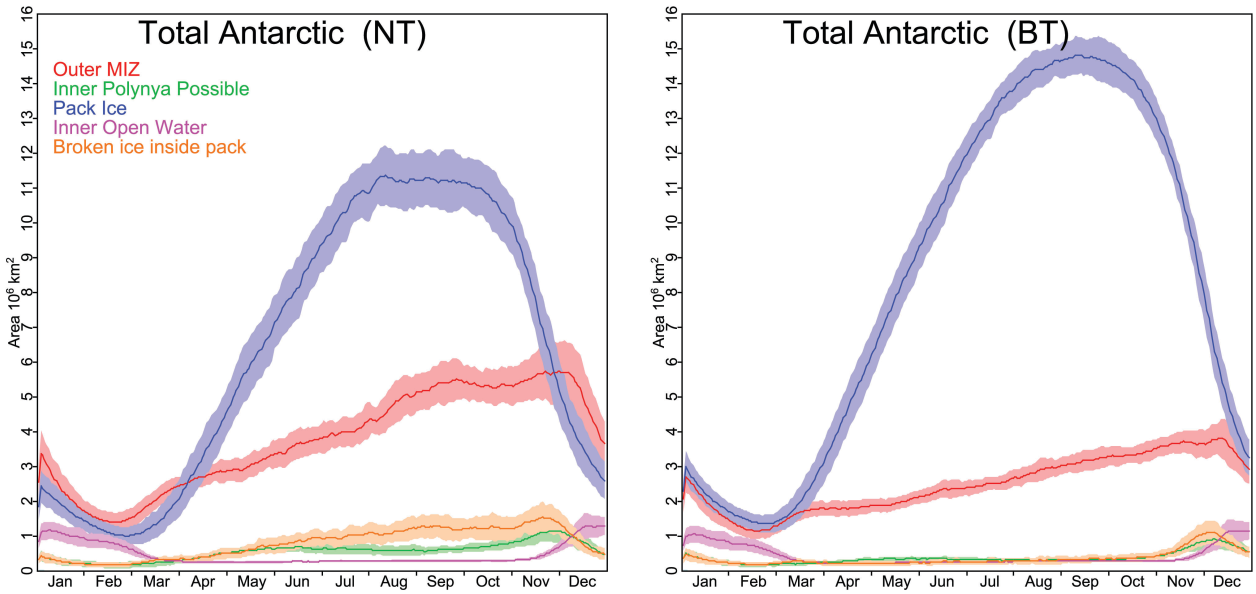

Figure 5. Long-term (1979-2014) and standard deviation (shading) of the seasonal cycle in total Antarctic extent of the consolidated pack ice, the outer marginal ice zone, polynyas, open pack ice (or broken ice within the pack ice), and inner open water. There are essentially no scattered ice floes outside of the MIZ. NASA Team results are shown on the left and the Bootstrap on the right.

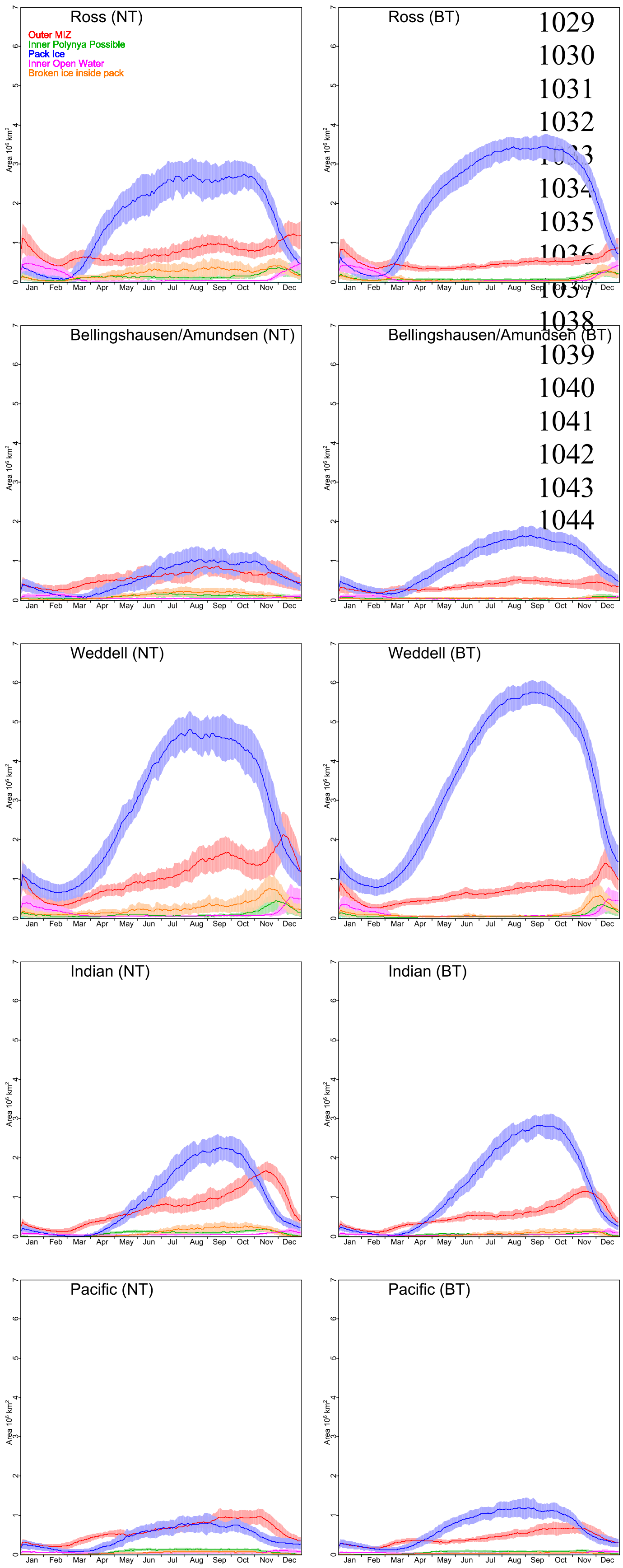

Figure 6. Long-term (1979-2014) seasonal cycle in regional sea ice extent of the consolidated pack ice, the outer marginal ice zone, polynyas, open pack ice (or broken ice within the pack ice), and inner open water. Results for the NASA Team algorithm are shown on the left and Bootstrap on the right, and for the Ross, Bellingshausen/Amundsen, Weddell, Indian and Pacific Oceans.

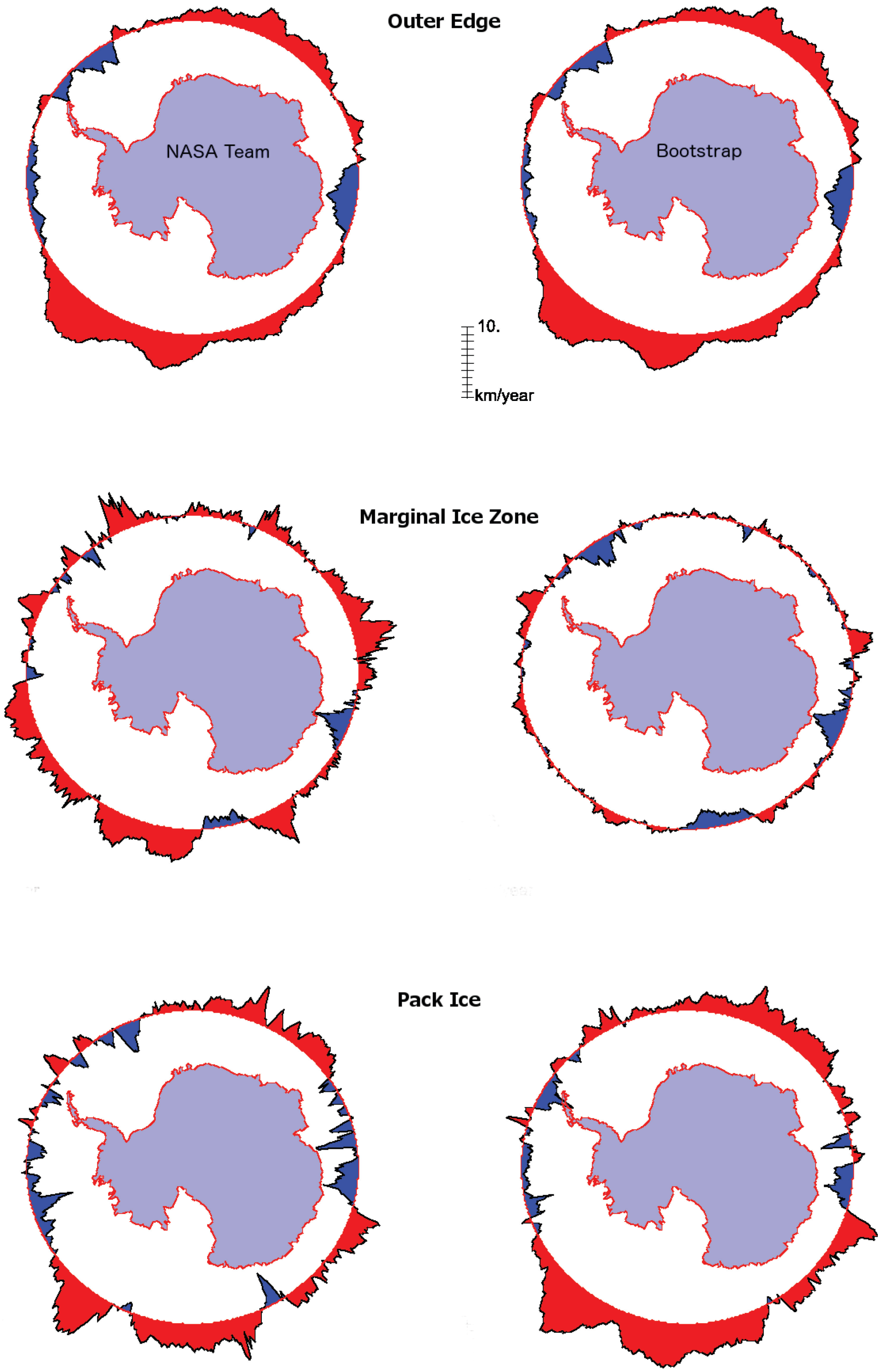

Figure 7. Expansion (red) or contraction (blue) of the outer ice edge (top), the width of the marginal ice zone (middle) and the width of the pack ice from 1979 to 2014 during the month of September relative to 60S.

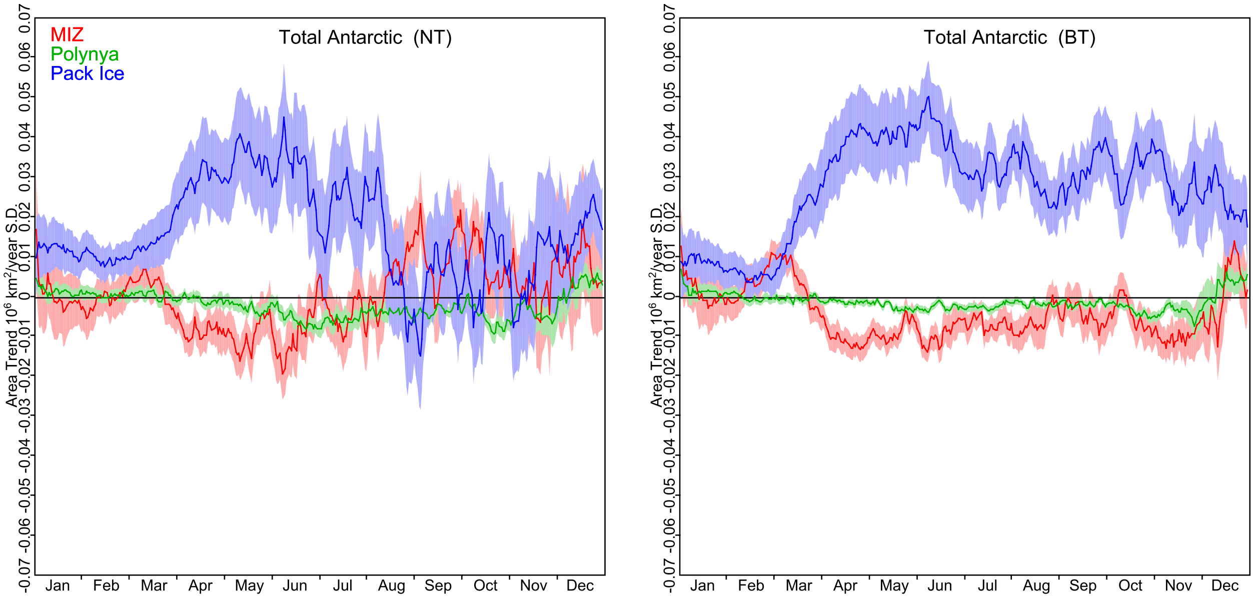

Figure 8. Daily trends (1979 to 2014) in the consolidated pack ice, the outer MIZ and potential coastal polynyas for the entire Antarctic sea ice cover for the NASA Team (left) and Bootstrap (right) algorithms. Trends are provided in 10^6 km^2 a^{-1}.

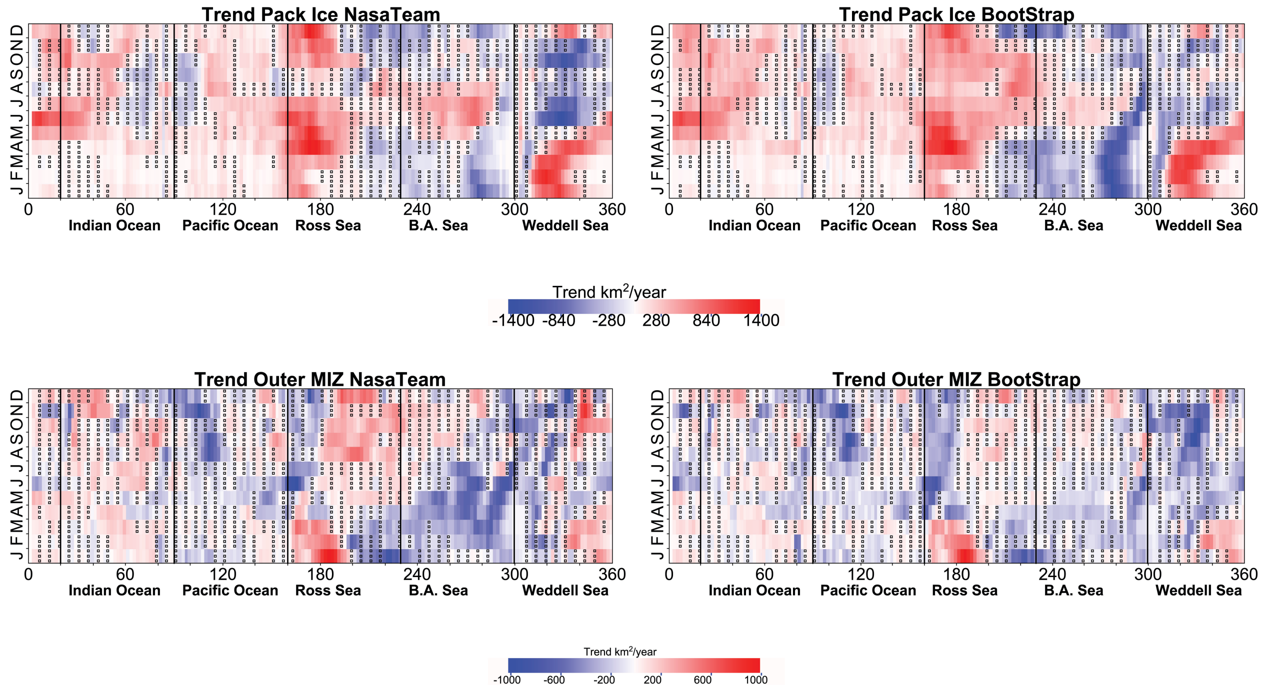

Figure 9. Daily (1979-2014) trends in regional sea ice extent of the consolidated pack ice (top) and the outer marginal ice zone (bottom). Results for the NASA Team algorithm (left) and Bootstrap (right) are shown as a function of longitude. Trends are provided in 10^6 km^2 a^{-1}. Note the difference in color bar scales. Regions not statistically significant are highlighted.

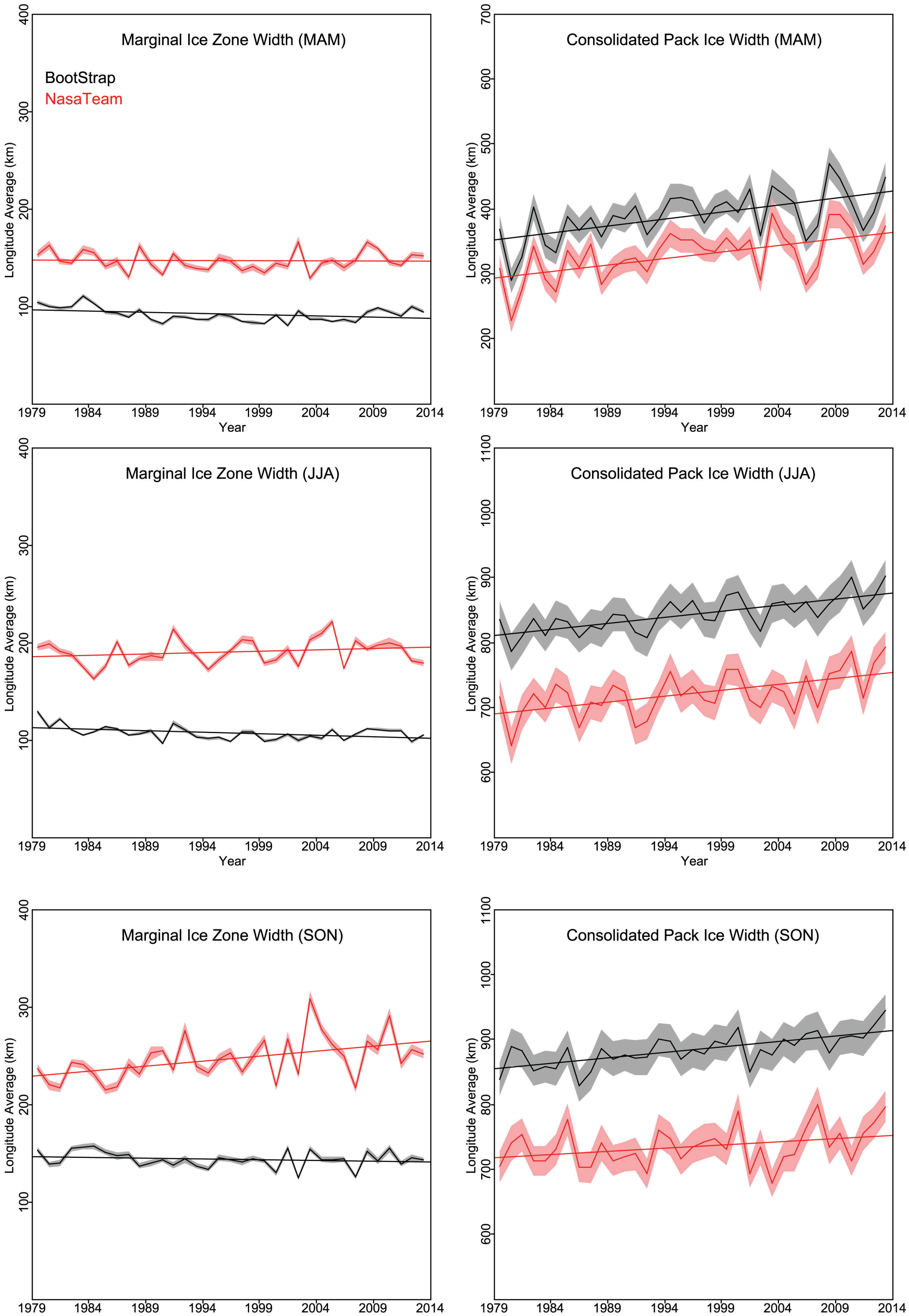

Figure 10. Time-series of seasonal mean MAM (top), JJA (middle) and SON (bottom) marginal ice zone (left) and consolidated pack ice (right) for both sea ice algorithms; NASA Team is shown in red, Bootstrap in black. Shading represents one standard deviation. Note the difference in y-axis between the pack ice and the MIZ plots.

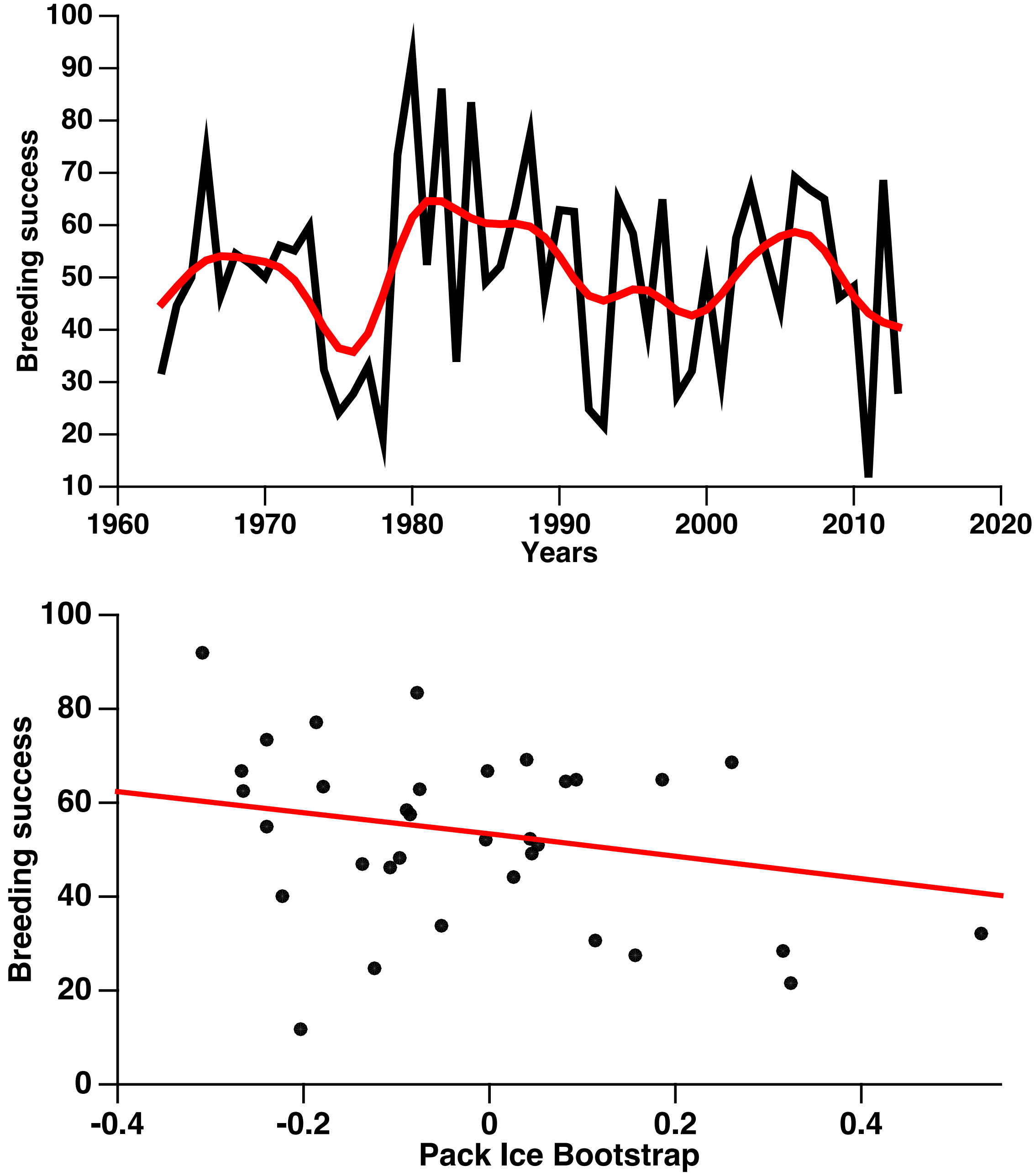

Figure 11. Breeding success of snow petrel (top) since the 1960s and the effect of the Bootstrap consolidated pack ice area (x-axis) on the breeding success of snow petrels (y-axis) (bottom).